NEOPLASIA
www.neoplasia.com

Volume 13 Number 11 November 2011 pp. 1043–1057 1043

A Novel Topoisomerase Inhibitor, Daurinol, Suppresses Growth of HCT116 Cells with Low Hematological Toxicity Compared to Etoposide[1,2]

Kyungsu Kang[*,†], Seung Hyun Oh[‡,§], Ji Ho Yun[*], Eun Hye Jho[*], Ju-Hee Kang[‡], Dulamjav Batsuren[¶], Jigjidsuren Tunsag[¶], Kwang Hwa Park[#], Minkyun Kim[†] and Chu Won Nho[*]

*Functional Food Center, Korea Institute of Science and Technology, Gangneung, Gangwon-do, Republic of Korea; [†]Department of Agricultural Biotechnology, Seoul National University, Seoul, Republic of Korea; [‡]Department of Cancer Experimental Resources Branch, National Cancer Center, Gyeonggi-do, Republic of Korea; [§]College of Pharmacy, Gachon University of Medicine and Science, Incheon, Republic of Korea; [¶]Institute of Chemistry and Chemical Technology, Ulaanbaatar, Mongolia; [#]Wonju Christian Hospital, Yonsei University, Gangwon-do, Republic of Korea

Abstract

We report that daurinol, a novel arylnaphthalene lignan, is a promising potential anticancer agent with adverse effects that are less severe than those of etoposide, a clinical anticancer agent. Despite its potent antitumor activity, clinical use of etoposide is limited because of its adverse effects, including myelosuppression and the development of secondary leukemia. Here, we comprehensively compared the mechanistic differences between daurinol and etoposide because they have similar chemical structures. Etoposide, a topoisomerase II poison, is known to attenuate cancer cell proliferation through the inhibition of DNA synthesis. Etoposide treatment induces G_2/M arrest, severe DNA damage, and the formation of giant nuclei in HCT116 cells. We hypothesized that the induction of DNA damage and nuclear enlargement due to abnormal chromosomal conditions could give rise to genomic instability in both tumor cells and in actively dividing normal cells, resulting in the toxic adverse effects of etoposide. We found that daurinol is a catalytic inhibitor of human topoisomerase IIα, and it induces S-phase arrest through the enhanced expression of cyclins E and A and by activation of the ATM/Chk/Cdc25A pathway in HCT116 cells. However, daurinol treatment did not cause DNA damage or nuclear enlargement *in vitro*. Finally, we confirmed the *in vivo* antitumor effects and adverse effects of daurinol and etoposide in nude mice xenograft models. Daurinol displayed potent antitumor effects without any significant loss of body weight or changes in hematological parameters, whereas etoposide treatment led to decreased body weight and white blood cell, red blood cell, and hemoglobin concentration.

Neoplasia (2011) 13, 1043–1057

Address all correspondence to: Chu Won Nho, PhD, Functional Food Center, Korea Institute of Science and Technology, Gangneung Institute, Gangneung, Gangwon-do 210-340, Republic of Korea. E-mail: cwnho@kist.re.kr; or Minkyun Kim, PhD, Department of Agricultural Biotechnology, Center for Agricultural Biomaterials, Research Institute for Agriculture and Life Sciences, Seoul National University, Seoul 151-921, Republic of Korea. E-mail: mkkim3@snu.ac.kr

[1]This work was supported by an intramural grant (2Z03480) from the Korea Institute of Science and Technology and a grant from the Center Project for Korea-Mongolia Science and Technology Cooperation (Ministry of Education, Science, and Technology, Korea; 2U04260).
[2]This article refers to supplementary materials, which are designated by Figures W1 to W8 and are available online at www.neoplasia.com.
Received 13 July 2011; Revised 8 September 2011; Accepted 19 September 2011

DOI 10.1593/neo.11972

Introduction

Myelosuppression, a decrease in blood cell production due to bone marrow cell abnormalities, is one of the most common and serious adverse effects of cancer chemotherapy [1]. Clinically, myelosuppression is characterized by hematological changes, such as a decrease in the number of red blood cells (anemia), white blood cells (leukopenia or neutropenia), and platelets (thrombocytopenia) [1,2]. Etoposide (VP-16), an aryltetraline lignan, is a clinical antitumor drug used to treat various human cancers, including small cell lung cancer and testicular cancer [3,4]. However, the adverse effects of etoposide reported in clinical trials include both myelosuppression and the development of secondary cancers, particularly etoposide-induced leukemia [2,3,5]. Etoposide-induced myelosuppression during cancer chemotherapy has also been reported in animal models [6], and combinatorial treatment with other chemical compounds, such as dexrazoxane, quercetin, and wongonin, has been performed to ameliorate etoposide-induced damage to bone marrow cells in animal studies [7–10].

Etoposide inhibits the activity of human topoisomerase IIα. It is classified as a topoisomerase II poison because it stabilizes the DNA-topoisomerase complex (also called the DNA cleavable complex) [11]. In contrast, a compound that interferes with at least one step of the catalytic cycle of topoisomerase II without the formation of the DNA cleavable complex is classified as a catalytic topoisomerase inhibitor [12]. By forming the DNA cleavable complex, etoposide induces severe genotoxic DNA damage in cancer cells and normal bone marrow cells [10,13]. Consequently, this genotoxic DNA damage increases aberrant DNA recombination events and accelerates abnormal chromosome rearrangements that seem to be connected to the adverse effects of etoposide [6,14]. Etoposide induces G_2/M phase arrest [15–17] as well as the formation of abnormally shaped giant cell and nuclei in various cancer cells, likely because cells cannot enter mitosis despite sufficient synthesis of DNA and proteins for cell division [18,19]. Thus, we hypothesized that the formation of giant nuclei and abnormal chromosomal rearrangements induced by etoposide treatment could be the main reasons for its toxic side effects. Therefore, chemicals with similar properties that do not induce DNA damage and nuclear enlargement may act as good clinical substitutes for etoposide, with fewer adverse effects.

Daurinol is a novel natural arylnaphthalene lignan whose structure is quite similar to etoposide. Daurinol is isolated from a traditional ethnopharmacological plant, *Haplophyllum dauricum*, which has historically been used to treat tumors in Russia [20,21]. The first report of daurinol isolation was published in 1981 [20], but its biological and pharmacological activity has never been investigated yet. Antiproliferative activities of arylnaphthalene lignans against various human cancer cells have been reported, but the molecular mechanism of their antiproliferative effects is still poorly elucidated [22–24].

Here, we propose that daurinol may be a novel alternative to the clinical anticancer agent etoposide. To support this, we compared the effects of daurinol and etoposide *in vitro* and *in vivo*. In addition, we characterized the detailed molecular mechanism of the anticancer activity of daurinol. This approach provides practical information for the development of anticancer agents with lower adverse effects, such as myelosuppression, and elucidates the molecular mechanism underlying the inhibition of cancer cell proliferation induced by this naturally occurring arylnaphthalene lignan.

Materials and Methods

Materials

Daurinol was isolated from the Mongolian medicinal plant *H. dauricum* as previously described [20]. Etoposide, propidium iodide, Cremophor, ethanol, and calf thymus DNA were purchased from Sigma (St Louis, MO). The chemical structures of daurinol and etoposide are shown in Figure 1*A*. Daurinol and etoposide were dissolved in dimethyl sulfoxide (DMSO) for cellular treatment *in vitro*. Human topoisomerase IIα was purchased from TopoGEN (Port Orange, FL). Antibodies against p-ATM (Ser1981) (4526), ATM (2873), p-Chk1 (Ser317) (2344), p-Chk1 (Ser345) (2341), Chk1 (2345), p-Chk2 (Thr68) (2661), Chk2 (2662), Cdc25A (3652), p-Cdc2 (Tyr15) (4539), Cdc2 (9112), E2F-1 (3742), cyclin A (4656), Cdk4 (2906), and cyclin D1 (2922) were purchased from Cell Signaling Technology (Danvers, MA). Antibodies against Cdk2 (sc-163), cyclin E (sc-247), and β-actin (sc-47778) were purchased from Santa Cruz Biotechnology (Santa Cruz, CA). The antibody against p-Cdk2 (Tyr15) (ab76146) was purchased from Abcam (Cambridge, United Kingdom). Secondary anti-rabbit and anti-mouse antibodies were purchased from Santa Cruz Biotechnology.

Cell Culture

SW480, DLD-1, and HCT116 human colorectal cancer; A549 human lung cancer; AGS human gastric cancer; HepG2 human liver cancer; and MCF-7 human breast cancer cell lines were obtained from the American Type Culture Collection (Rockville, MD). HCT116, DLD-1, and MCF-7 cells were cultured in minimal essential medium (MEM) supplemented with 10% fetal bovine serum (FBS), 100 U/ml penicillin, and 100 μg/ml streptomycin. A549, AGS, and SW480 cells were maintained in Roswell Park Memorial Institute 1640 medium supplemented with 25 mM HEPES, 10% FBS, 100 U/ml penicillin, and 100 μg/ml streptomycin. HepG2 cells were cultured in Dulbecco modified Eagle medium supplemented with 10% FBS, 100 U/ml penicillin, and 100 μg/ml streptomycin. Cells were cultured in a humidified atmosphere (95% air, 5% CO_2) at 37°C.

Figure 1. Daurinol inhibits cell proliferation and DNA synthesis. (A) Chemical structures of daurinol and etoposide. (B) Antiproliferative activity of daurinol was determined by cell viability assays in various human cancer cell lines. Cells were treated with various concentrations of daurinol for 24 and 48 hours. IC_{50}, the concentration that inhibits 50% of cell proliferation. Means ± SD from three independent experiments are shown. (C) Inhibition of cell viability and DNA synthesis by treatment with daurinol or etoposide for 24 and 48 hours was determined by CCK-8 assay (mitochondrial dehydrogenase activity) and BrdU incorporation ELISA in HCT116 cells. Cell viability (%) and BrdU incorporation (%) were calculated as percents of the vehicle control. Data are expressed as mean ± SD from triplicate experiments. $^{**}P < .01$ and $^{***}P < .001$, for significant differences from the vehicle control. Graphs are representative of three independent experiments. (D) Cell viability *versus* BrdU incorporation (left). Relative DNA synthesis was calculated by BrdU incorporation (%) over cell viability (%) (right). Columns and error bars indicate mean ± SD. $^{*}P < .05$, $^{**}P < .01$, and $^{***}P < .001$, for significant differences from the vehicle control. Graphs are representative of three independent experiments.

Measurement of Cell Viability and DNA Synthesis

To measure the antiproliferative activity of daurinol in various cancer cell lines, cell viability was determined by measurement of mitochondrial dehydrogenase activity using a Cell Counting Kit (CCK-8) purchased from Dojindo Laboratories (Tokyo, Japan), as previously described [25]. Briefly, cancer cells (5×10^3 cells per well) were plated in 96-well plates, incubated at 37°C for 24 hours, and treated with 0 to 100 μM daurinol for 24 and 48 hours.

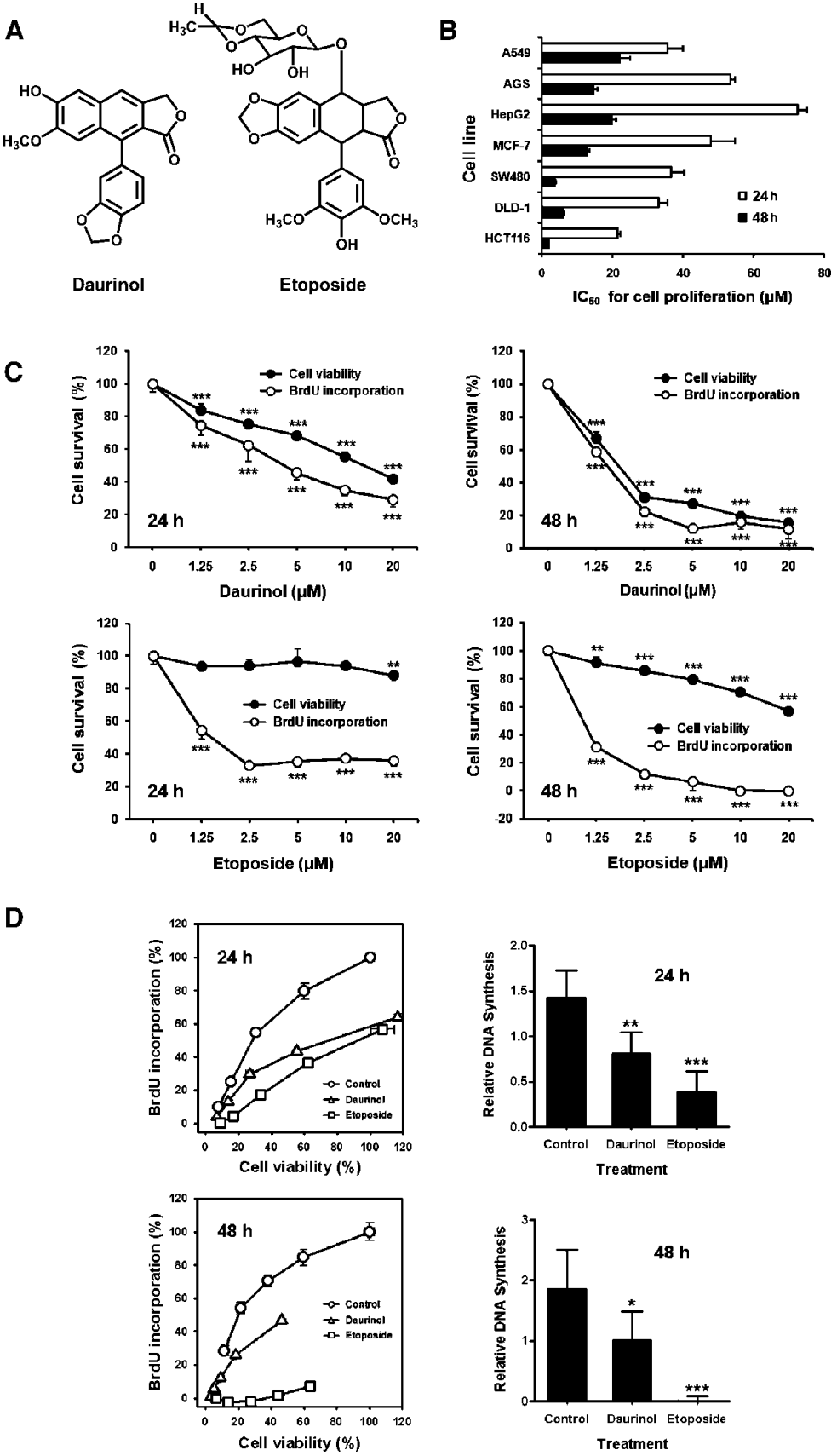

We also measured the cell viability and DNA synthesis of HCT116 and DLD-1 cells treated with daurinol or etoposide using CCK-8 assays and 5-bromo-2′-deoxyuridine (BrdU) incorporation enzyme-linked immunosorbent assay (ELISA), respectively. BrdU incorporation was measured using a Cell Proliferation ELISA BrdU Kit (Roche, Mannheim, Germany) according to the manufacturer's instructions. Briefly, HCT116 and DLD-1 cells (5×10^3 cells per well) were plated in 96-well plates, incubated at 37°C for 24 hours, and treated with 1.25 to 20 μM daurinol or etoposide for 24 and 48 hours. The BrdU labeling solution was added during the last 2 hours of the treatment. Cell survival (%) and BrdU incorporation (%) were calculated as the percentage of the absorbance at 450 nm of chemical-treated cells compared to control cells treated with only DMSO.

BrdU incorporation measured by ELISA may decrease owing to the inhibition of DNA synthesis or decreased cell viability. To solve this problem, we measured both the BrdU incorporation and cell viability of our cell lines at different stages of confluence. We plated different numbers of HCT116 and DLD-1 cells (6.25×10^2, 1.25×10^3, 2.5×10^3, 5×10^3, and 1×10^4 cells per well) in 96-well plates, incubated at 37°C for 24 hours, and treated with 5 μM daurinol or 10 μM etoposide for 24 and 48 hours. The CCK-8 cell viability assay and BrdU labeling solutions were added during the last 2 hours of the treatment. Then, cell viability and BrdU incorporation were determined using spectrophotometry. We calculated the relative DNA synthesis as the percentage of BrdU incorporation (%) over cell viability (%).

Cell Cycle Analysis

Cell cycle profiles were obtained by DNA content analysis using a flow cytometer (Becton Dickinson, San Jose, CA) and Modfit LT 3.0 software, as previously described [25]. Briefly, HCT116 and DLD-1 cells (5×10^5 cells) were seeded in 60-mm dishes, incubated for 24 hours, and treated with 0 to 10 μM daurinol for 24 to 72 hours. We also confirmed the effect of daurinol on cell cycle progression in HCT116 cells in both G_0/G_1 and G_1/S synchronized conditions. For G_0/G_1 phase synchronization, HCT116 and DLD-1 cells (2×10^5) were seeded on 60-mm dishes, incubated at 37°C for 24 hours, and pretreated with serum-free MEM for 24 hours. Then, 0 to 10 μM daurinol was added for 24 and 48 hours in normal MEM containing 10% FBS. For G_1/S–phase synchronization, HCT116 and DLD-1 cells (2×10^5) were seeded on 60-mm dishes, incubated at 37°C for 24 hours, and pretreated with 2 mM hydroxyurea for 12 hours. Cells were washed twice with Dulbecco phosphate-buffered saline (DPBS) and once with medium to remove the residual hydroxyurea. Then, 0 to 10 μM daurinol was added for 12, 24, and 48 hours. Both floating and adherent cells were harvested by trypsinization and fixed in 70% ethanol at −20°C for at least 1 day. Cells were stained with propidium iodide, and their DNA contents were analyzed by flow cytometry.

Topoisomerase IIα Inhibition Assay

The inhibitory activity of daurinol and etoposide against human topoisomerase IIα was measured by *in vitro* biochemical assay using a Topoisomerase II Drug Screening Kit (TopoGEN). The standard reaction mixture (20 μl) contained 50 mM Tris-HCl (pH 8.0), 150 mM NaCl, 10 mM $MgCl_2$, 0.5 mM dithiothreitol, 30 μg of bovine serum albumin, 2 mM ATP, 375 ng of supercoiled DNA (pHOT1), 2 μl of topoisomerase IIα, and 2 μl of tested compound dissolved in DMSO. The reaction mixture was incubated at 37°C for 30 minutes, and 2 μl of 10% sodium dodecyl sulfate was added to stop the reaction. Then, proteinase K (50 μg/ml final concentration) was added, and the reactions were incubated for an additional 15 minutes to remove topoisomerase IIα from the DNA. The reaction mixtures were cleaned by extraction with a 25:24:1 phenol-chloroform-isoamyl alcohol solution. DNA relaxation was evaluated by agarose gel electrophoresis both in the presence and in the absence of ethidium bromide. The DNA samples were electrophoresed through 1% agarose gels at 1.7 V/cm for 30 minutes in 40 mM Tris-acetate and 1 mM EDTA buffer and imaged with an i-MAX Gel Image Analysis System (Core Bio System, Seoul, Republic of Korea).

Comet Assay

DNA damage was evaluated using single-cell gel electrophoresis with a Trevigen kit (Gaithersburg, MD), as previously described [26]. Briefly, HCT116 cells (3×10^5 cells per well) were plated in six-well plates, incubated for 24 hours, and treated with 0 to 50 μM daurinol or 10 μM etoposide for 6 hours. Cells were harvested by trypsinization and resuspended in ice-cold DPBS. Then, cells (2×10^3) were mixed with 100 μl of low-melting agarose at 37°C, spread on slides precoated with normal agarose, and solidified in the dark for 30 minutes at 4°C. Slides were lysed in ice-cold lysis solution in the dark for 50 minutes at 4°C and then incubated in an alkaline solution (pH > 13) at room temperature for 40 minutes to allow alkaline unwinding. Electrophoresis was performed under alkaline conditions for 50 minutes at 1 V/cm in a cold room (4°C). Slides were washed twice with distilled water, once with 70% ethanol, and stained with 2.5 μg/ml propidium iodide in distilled water for 20 minutes. Comet images were obtained using a fluorescence microscope (TE2000U; Nikon, Kanawa, Japan), and percent DNA in tail was calculated using TriTek CometScore 1.5 software (Sumerduck, VA).

Measurement of Interaction between Daurinol and DNA

Interaction between daurinol and DNA was evaluated by fluorescence quenching experiment. The absorption spectrum of daurinol dissolved in DPBS with 1% DMSO was obtained using a UV-visible spectrophotometer (Lamda35; PerkinElmer, Waltham, MA). Fluorescence spectra were recorded on a microplate reader (Infinite M1000; Tecan, Männedorf, Switzerland) at room temperature in the range of 400 to 650 nm with an excitation wavelength of 260 nm. The concentration of calf thymus DNA was determined according to the absorbance at 260 nm using the molar absorption coefficient (ε_{DNA}) 6600/M/cm. To measure the fluorescence emission spectrum, daurinol was dissolved in DPBS with 1% DMSO. For the fluorescence quenching experiment, 30 μM daurinol and different concentrations of calf thymus DNA (0-3.9 mM) were dissolved in DPBS with 1% DMSO. The Stern-Volmer quenching constant (K_{SV}) was calculated according to the Stern-Volmer equation:

$$F_0 / F = 1 + K_{SV}[DNA]$$

where F_0 and F are the fluorescence intensity in the absence and presence of DNA (quencher), respectively.

Measurement of Nuclear Size

Cellular morphologic changes after treatment with daurinol or etoposide were observed by differential interference contrast microscopy using a fluorescence microscope (TE2000U; Nikon). Changes of nuclei sizes were evaluated by fluorescent microscopy and flow cytometric fluorescence pulse width analysis (FL2-W) after cells were stained with

propidium iodide, according to previously described methods [18]. HCT116 cells (5×10^5 cells) were seeded on 60-mm dishes, incubated for 24 hours, and then treated with 0 to 10 μM daurinol or 10 μM etoposide for 24 and 48 hours.

Western Blot Analysis

HCT116 cells (5×10^5) were seeded on 60-mm dishes, incubated for 24 hours, and then treated with 5 μM daurinol for 2, 12, 24, and 48 hours. Additional procedures were performed as previously described [27]. Relative protein expression was measured by densitometry.

Mouse Tumor Xenografts and Treatments

Five-week-old athymic male nude mice (BALB/c *Slc-nu*) were purchased from SLC, Inc (Shizuoka, Japan). The mice were maintained in ventilated caging with a 12-hour light/12-hour dark photoperiod. Sterile food pellets (Teklad-certified irradiated global 18% protein rodent diet 2918C; Harlan Teklad) and water were provided *ad libitum*.

Tumor xenografts were established by subcutaneous injection of 1×10^7 HCT116 cells and maintained by serial transplantation. Tumor fragments ($3 \times 3 \times 3$ mm^3) were subcutaneously transplanted to the left lateral flank of athymic mice. Tumor volumes were measured using calipers and the formula $V = 0.5 \times \text{length} \times \text{width}^2$. When the tumor volume reached approximately 110 mm^3, mice were randomized into treatment groups of 10 animals per group. Two independent experiments were performed. The first experiment was performed to evaluate toxicity, antitumor activity, and their persistence of daurinol and etoposide. Mice were treated by intraperitoneal injection of solvent (4.2% DMSO, 10.4% Cremophor, 10.4% ethanol, and 75% PBS), daurinol (1, 5, 10, and 20 mg/kg), or etoposide (20 mg/kg) three times weekly for 2 weeks. Mice were then maintained for additional 2 weeks. Body weight and tumor volume were measured twice a week. On day 29, mice were killed, and tumors were removed and photographed. The second round of experiments was performed to confirm antitumor activity and to investigate changes in hematological parameters, protein expression, and histology. Mice were treated by intraperitoneal injection of solvent (4.2% DMSO, 10.4% Cremophor, 10.4% ethanol, and 75% PBS), daurinol (5, 10, and 20 mg/kg), or etoposide (20 mg/kg) twice weekly for 3 weeks. Body weight was measured twice a week, and tumor volume was measured three times a week. On day 18, mice were killed, and tumors were removed for BrdU immunohistochemistry and Western blot analysis. BrdU labeling was performed by the intraperitoneal injection of 0.2 ml of BrdU solution (5 mg/ml; Sigma) 2 hours before harvesting tumors. Kidney, colon, liver, and femur were also removed and fixed in 10% neutral-buffered formalin (BBC Biochemical, Mount Vernon, WA) for histologic analysis.

Histology and BrdU Immunohistochemistry

The fixed tumor, bone marrow, colon, kidney, and liver tissues were decalcified (femur), embedded in paraffin, and used for hematoxylin and eosin staining. For BrdU immunohistochemistry, the unstained tumor slides were incubated in 0.3% H_2O_2 for 30 minutes to block endogenous peroxidase activity. Antigen retrieval was performed by heating slides in 10 mM citrate buffer (pH 6.0) for 6 minutes and washing three times with PBS. Then, slides were incubated in the blocking agent (Immunotech, Marseille, France) for 1 hour and incubated with mouse anti-BrdU antibody (Dako, Glostrup, Denmark) in antibody dilution buffer (Immunotech) for 1 hour at room temperature. Slides were incubated with secondary antibody conjugated with peroxidase (Immunotech) for 10 minutes. Then, the color-producing reaction was performed using 3,3′-diaminobenzidine (DAB; Dako) for 15 minutes. The slides were counterstained with hematoxylin, and stained slides were visualized by light microscopy. Hematoxylin- and BrdU-positive cells were counted in three marginal areas of tumors for each individual ($n = 10$), and the percentage of BrdU-positive cells was calculated.

Hematological Parameter Analysis

Blood samples were collected from the abdominal vein and stored in EDTA-coated tubes (Becton Dickinson, Franklin Lakes, NJ). Hematological parameters were immediately determined using an Avida120 hematology analyzer (Siemens, Munich, Germany).

Statistical Analyses

Statistical analyses were performed by one-way analysis of variance followed by the Dunnett multiple comparison test or the Tukey multiple comparison test using GraphPad Prism 5 software (GraphPad Software, Inc, La Jolla, CA). $P < .05$ was considered statistically significant. Kolmogorov-Smirnov statistics were used to compare the distributions of two histogram plots obtained by flow cytometry [28].

Results

Daurinol Inhibits Cancer Cell Proliferation

First, we tested the ability of daurinol to inhibit cell proliferation in various human cancer cells by measurement of mitochondrial dehydrogenase activity. Daurinol displayed a potent antiproliferative effect on various human cancer cells with IC_{50} values (concentration that inhibits 50% of cell proliferation) below 20 μM after 48 hours of treatment (Figure 1*B*). Daurinol demonstrated the greatest antiproliferative activity in human colorectal cancer HCT116 cells, with IC_{50} values of 23.19 ± 0.67 at 24 hours and 2.03 ± 0.18 μM at 48 hours of treatment (Figure 1*B*). Therefore, we chose HCT116 cells as a model cell line in which to investigate the molecular mechanism of the antiproliferative effect of daurinol.

Daurinol Inhibits DNA Synthesis in HCT116 Cells

We hypothesized that the antiproliferative activity of daurinol was due to the inhibition of DNA synthesis. To test this, we measured cell viability and DNA synthesis after treatment with daurinol using CCK-8 and BrdU incorporation assays. Daurinol significantly inhibited cell viability (mitochondrial dehydrogenase activity) and BrdU incorporation (DNA synthesis) in HCT116 cells at all concentrations tested (1.25-20 μM). Etoposide was a more potent inhibitor of DNA synthesis (BrdU incorporation) than cell viability (mitochondrial dehydrogenase activity; Figure 1*C*). To confirm whether the decrease in BrdU incorporation by daurinol was due to blocking DNA synthesis rather than decreased cell viability by other cytotoxic effects, we performed an additional experiment in which we measured cell viability and BrdU incorporation at the same time in HCT116 cells at different levels of confluence after treatment with 5 μM daurinol or 10 μM etoposide and plotted cell viability *versus* BrdU incorporation. We then estimated the inhibition of DNA synthesis based on the distribution of the data. Both daurinol and etoposide displayed reduced BrdU incorporation rather than reduced cell viability compared to the vehicle control. The relative DNA synthesis indices (the percentage of BrdU incorporation by cell viability) of daurinol and etoposide were significantly lower than that of the vehicle control at both 24 and 48 hours of treatment (Figure 1*D*). We also measured cell viability and BrdU

incorporation in another colon cancer cell line, DLD-1, and found similar inhibitory activity (Figure W1). Taken together, we concluded that daurinol is a potent natural inhibitor of DNA synthesis.

Daurinol Induces S-phase Arrest in HCT116 Cells

Next, we investigated the effect of daurinol on the cell cycle progression of HCT116 cells using flow cytometric DNA content analysis. Daurinol (5 μM) induced S-phase arrest at 24, 48, and 72 hours of treatment (Figure 2*A*) in a dose-dependent manner (Figure 2*B*). We confirmed daurinol-induced S-phase arrest under G_1/S synchronized conditions via hydroxyurea synchronization (Figure 2*C*) and under G_0/G_1 synchronization conditions via serum starvation (data not shown), as described in Materials and Methods. We also observed that daurinol induced S-phase arrest in DLD-1 cells (Figure W2). Because DNA replication occurs during the S-phase, we assumed that daurinol-induced S-phase arrest was due to the abrogation of DNA replication by the inhibitory activity of daurinol. Etoposide is known to be a potent

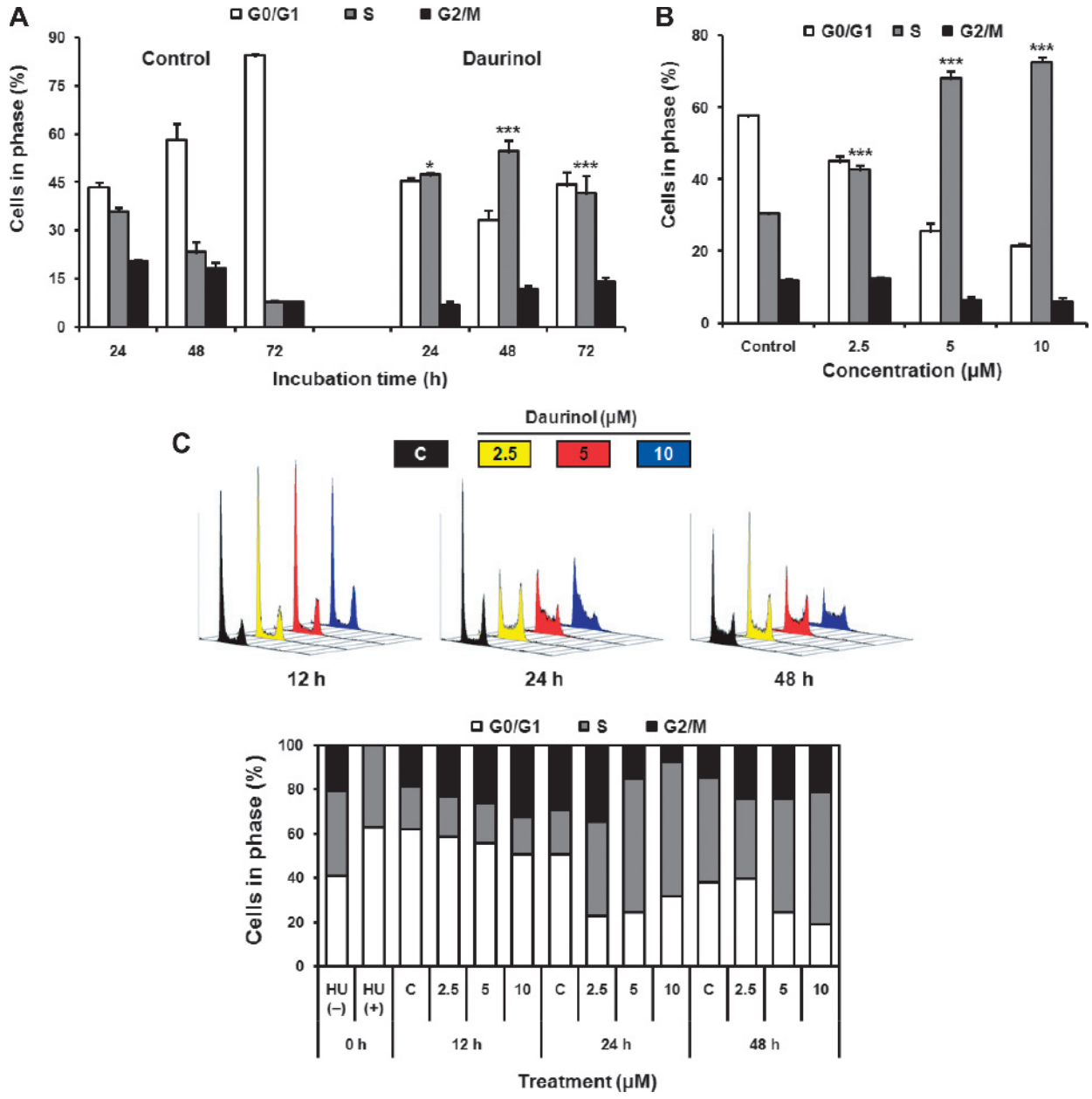

Figure 2. Daurinol induces S-phase arrest in HCT116 cells. Cell cycle distribution was evaluated by using flow cytometric DNA content analysis. (A) HCT116 cells were treated with 5 μM daurinol for 24, 48, and 72 hours. Columns and error bars indicate mean ± SD from triplicate experiments. *$P < .05$ and ***$P < .001$, for significant differences from the vehicle control at each treatment time. The graph is representative of three independent experiments. (B) HCT116 cells were treated with various concentrations of daurinol (0, 2.5, 5, and 10 μM) for 48 hours. Columns and error bars indicate mean ± SD from quadruplicate experiments. ***$P < .001$, for significant differences from the vehicle control. (C) Daurinol-induced S-phase arrest of HCT116 cells was confirmed in hydroxyurea-synchronized cells. Cells were pretreated with 2 mM hydroxyurea (HU) for 12 hours to synchronize in the G_1/S–phase. Then, cells were treated with daurinol (0, 2.5, 5, and 10 μM) for 12, 24, and 48 hours. C indicates vehicle control. The graph is representative of three independent experiments.

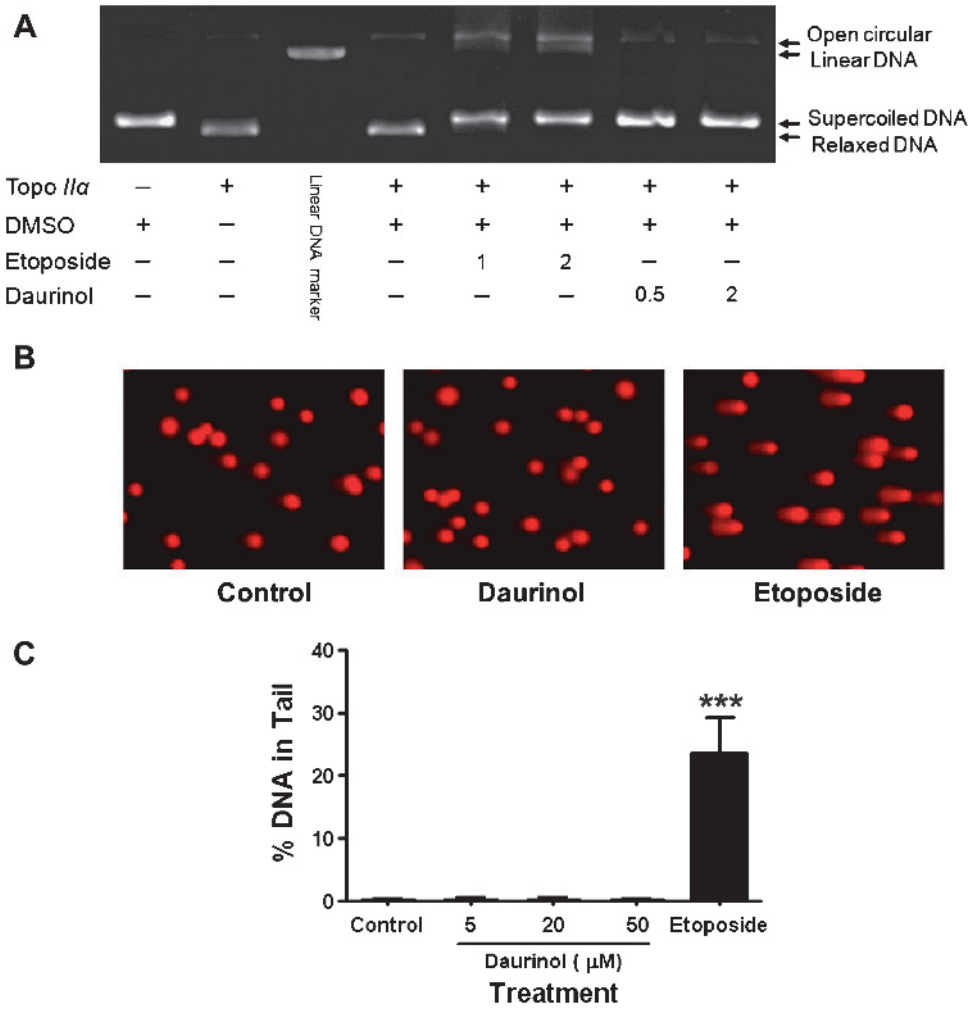

Figure 3. Daurinol is a catalytic inhibitor of human topoisomerase IIα. (A) Inhibitory activity of daurinol and etoposide on human topoisomerase IIα was evaluated by *in vitro* biochemical assays. The supercoiled DNA (pHOT1) substrate was incubated with human topoisomerase IIα in the presence of daurinol (1 and 2 mM) or etoposide (0.5 and 2 mM). DNA relaxation was evaluated by 1% agarose gel electrophoresis in the presence of ethidium bromide. (B and C) Effects of daurinol and etoposide on DNA damage were determined by comet assays. HCT116 cells were treated with daurinol (5, 20, and 50 μM) or 10 μM etoposide for 6 hours. (B) Images of cellular DNA damage were detected by fluorescence microscopy. Pictures are representative of three independent experiments. (C) The DNA damage index (% DNA in tail) was determined using comet score software. Columns and error bars indicate mean ± SD ($n = 50$). ***$P < .001$, for significant differences from the vehicle control.

agent for the induction of G_2/M–phase arrest in various cancer cells [4,12,18,29]. This difference in phases of cell cycle blockage was the first noticeable distinction between daurinol and etoposide, although both are inhibitors of DNA synthesis.

Daurinol Is a Catalytic Inhibitor of Human Topoisomerase IIα

We next examined the inhibitory activity of daurinol against human topoisomerase IIα using an *in vitro* biochemical assay that measures the relaxation of supercoiled DNA. Etoposide is a well-known topoisomerase poison, and it stabilizes the DNA cleavable complex [13]. Both etoposide and daurinol inhibited human topoisomerase IIα, preventing unwinding of the supercoiled DNA substrate (Figures 3*A* and W3). As previously reported [13], etoposide induced the formation of open circular and linear DNA, which originated from the topoisomerase-DNA cleavable intermediate, but daurinol did not give rise to any open circular or linear DNA (Figure 3*A*).

We also measured DNA damage after treatment with daurinol or etoposide in HCT116 cells using comet assays. Etoposide (10 μM) clearly induced the formation of comet tails, indicating that etoposide significantly induces DNA damage (% DNA in tail). In contrast, even 50 μM daurinol did not induce the formation of DNA comet tails (Figure 3, *B* and *C*). Because the formation of comet tails implies severe DNA damage in cells, we concluded that DNA damage induced by etoposide treatment is much greater than that of daurinol. The formation of comet tail occurs when the DNA cleavable complex is formed in cells, which is an important property of topoisomerase poisons [30]. Therefore, we concluded that daurinol must be a catalytic inhibitor of human topoisomerase IIα rather than a topoisomerase poison because treatment with daurinol induces less DNA damage compared to the etoposide treatment. This was the second key distinction between daurinol and etoposide.

We also measured the biophysical interaction between daurinol and DNA using fluorescence quenching experiments to test whether

catalytic inhibition of topoisomerase by daurinol involves an actual interaction between daurinol and DNA. Through UV-visible spectroscopy, we determined that daurinol has an absorbance maximum at 259.4 nm (Figure W4). Daurinol emitted fluorescence at 480 nm with an excitation wavelength of 260 nm. The fluorescence intensity of daurinol displayed a linear relationship with its concentration (Figure W5*B*), confirming that the fluorescence was emitted from daurinol. On addition of calf thymus DNA, the fluorescence of daurinol was efficiently quenched (Figure W5*C*). Theoretically, quenching of daurinol fluorescence is due to the physical interaction between daurinol and DNA (Figure W5*A*). We calculated the Stern-Volmer quenching constant (K_{SV}), which indicates the interaction strength between biomolecules, using the Stern-Volmer equation and found that the K_{SV} was 635.7 ± 60.2 M^{-1} (Figure W5*D*). This interaction intensity was comparable to that of quinolone antibiotics, *R*-ofloxacin (746 M^{-1}) and synthetic alkaloids, luotonin A derivatives (571-945 M^{-1}) [31,32]. We speculated that the interaction of daurinol and DNA may at least partially contribute to the inhibition of topoisomerase and DNA synthesis.

Daurinol Induces S-phase Arrest through Enhanced Expression of Cyclins E and A and Activation of the ATM/Chk/Cdc25A Pathway

To elucidate the molecular mechanism underlying the cell cycle block induced by daurinol, we examined the phosphorylation state and expression of cell cycle regulatory proteins in HCT116 cells treated with daurinol. First, we investigated cyclin E and cyclin A expression because Cdk2/cyclin E and Cdk2/cyclin A complexes are involved in the initiation and progression of the S-phase, respectively [33–35]. The expression of cyclin E rapidly increased at early times (12 and 24 hours) of the daurinol treatment compared with the vehicle control (Figure 4, *A* and *I*). The expression of cyclin A was significantly increased at 24 and 48 hours after daurinol treatment (Figure 4, *A* and *J*). In addition, the expression of E2F-1 was significantly increased at 24 hours after treatment (Figure 4, *A* and *H*). We also investigated the ATM/Chk/Cdc25A pathway, which is an important signaling pathway that regulates the DNA replication and DNA damage checkpoint. Treatment with daurinol activated this pathway at late time points (24 and 48 hours), as the phosphorylation levels of ATM at Ser1981, Chk1 at Ser317 and Ser345, and Chk2 at Thr68 were significantly increased (Figure 4, *A–E*). Expression of Cdc25A was also significantly decreased at 48 hours (Figure 4, *A* and *K*). Cdc25A is a downstream signaling component of Chk1/2 [33,36,37] and a signaling phosphatase that activates Cdk2 and Cdc2 by dephosphorylating their Tyr15 residues, which is important for cyclin-dependent kinase regulation of G_1/S (Cdk2) and G_2/M transitions (Cdc2) [36,38]. We also observed an increase in the phosphorylation of Cdk2 at Tyr 15 and Cdc2 at Tyr15 (Figure 4, *A* and *F* and *G*), suggesting that daurinol inhibits the G_1/S and G_2/M checkpoints.

In Contrast to Etoposide, Daurinol Does Not Induce a Nuclear Enlargement in HCT116 Cells

Etoposide induces the formation of giant cells and nuclei in cancer cells, including HCT116 cells [18,32]. Observations using differential interference contrast microscopy revealed that 48 hours of daurinol treatment does not induce changes in cell and nuclear enlargement, as seen after etoposide treatment (Figure W6). We also measured nuclear size after treatment with daurinol using fluorescent microscopy and fluorescence pulse width analysis. Fluorescence microscopic observation and quantification of nuclear size using the circle measurement algorithm of the microscope software revealed that daurinol does not trigger nuclear enlargement compared to the vehicle control. Nuclear sizes in daurinol-treated cells were similar to vehicle control cells, whereas those of etoposide-treated cells were significantly larger (Figure 5, *A–C*). Flow cytometric pulse width analysis also demonstrated that daurinol treatment does not induce a significant enlargement of cells or nuclei, as opposed to etoposide treatment. The FSC-H and FL2-W values (which refer cell size and nuclear size, respectively) of the daurinol-treated cells had a similar distribution to vehicle-treated control cells, whereas etoposide-treated cells occupied much higher positions than controls (Figure 5*D*). The mean values of FSC-H (which refers to cell size) were 418.8 ± 22.0 for the vehicle control, 411.8 ± 9.4 for 5 μM daurinol-treated cells, and 544.0 ± 11.8 for 10 μM etoposide-treated cells at 48 hours. The mean values of FL2-W (which refers to nuclear size) were 207.1 ± 0.5 for the vehicle control, 203.2 ± 0.8 for 5 μM daurinol, and 322.6 ± 3.1 for 10 μM etoposide treatments. We also compared distributions on histogram plots using Kolmogorov-Smirnov statistics, which estimate the differential distribution of two histogram plots. The $D/s(n)$ (the index of similarity) values of the daurinol-treated cells (2.5, 5, 10 μM for 48 hours) compared to vehicle control cells were significantly lower than those of etoposide-treated cells (10 μM for 48 hours; Figure 5*E*). Changes in nuclear size after treatment with daurinol and etoposide were also measured at 24 hours after treatment and were similar to the results of the 48-hour treatment (Figure W7).

This was the third crucial distinction between daurinol and etoposide. This difference between the effects of daurinol and etoposide may be the most important for chemotherapeutic applications. We hypothesized that the adverse effects of etoposide might originate from the abnormal nuclear enlargement that is caused by severe DNA damage and G_2/M arrest. Therefore, we hypothesized that daurinol would have fewer adverse effects because it does not induce significant nuclear enlargement, as it can induce S-phase arrest without causing severe DNA damage.

Daurinol Exerts Antitumorigenic Effects in Nude Mice Xenografts

To test our hypothesis about the severity of daurinol adverse effects *in vivo*, we investigated the antitumor effects and adverse effects of daurinol and etoposide treatment in mice. Two independent *in vivo* experiments were performed using a nude mice xenograft model. The

Figure 4. Effect of daurinol on the expression and phosphorylation of cell cycle regulatory proteins. HCT116 cells were treated with 5 μM daurinol for 2, 12, 24, and 48 hours. (A) Representative immunoblots are shown from three independent experiments. The relative expression of p-ATM (Ser1981)/ATM (B), p-Chk1 (Ser317)/Chk1 (C), p-Chk1 (Ser345)/Chk1 (D), p-Chk2 (Thr68)/Chk2 (E), p-Cdk2 (Tyr15)/Cdk2 (F), p-Cdc2 (Tyr15)/Cdc2 (G), E2F-1/β-actin (H), Cyc E/β-actin (I), Cyc A/β-actin (J), Cdc25A/β-actin (K), Cdk4/β-actin (L), and Cyc D1/β-actin (M) were determined by densitometry. Columns and error bars indicate mean ± SEM from three independent experiments. *$P < .05$, **$P < .01$, and ***$P < .001$ for significant differences between the vehicle control and daurinol-treated cells at each time point.

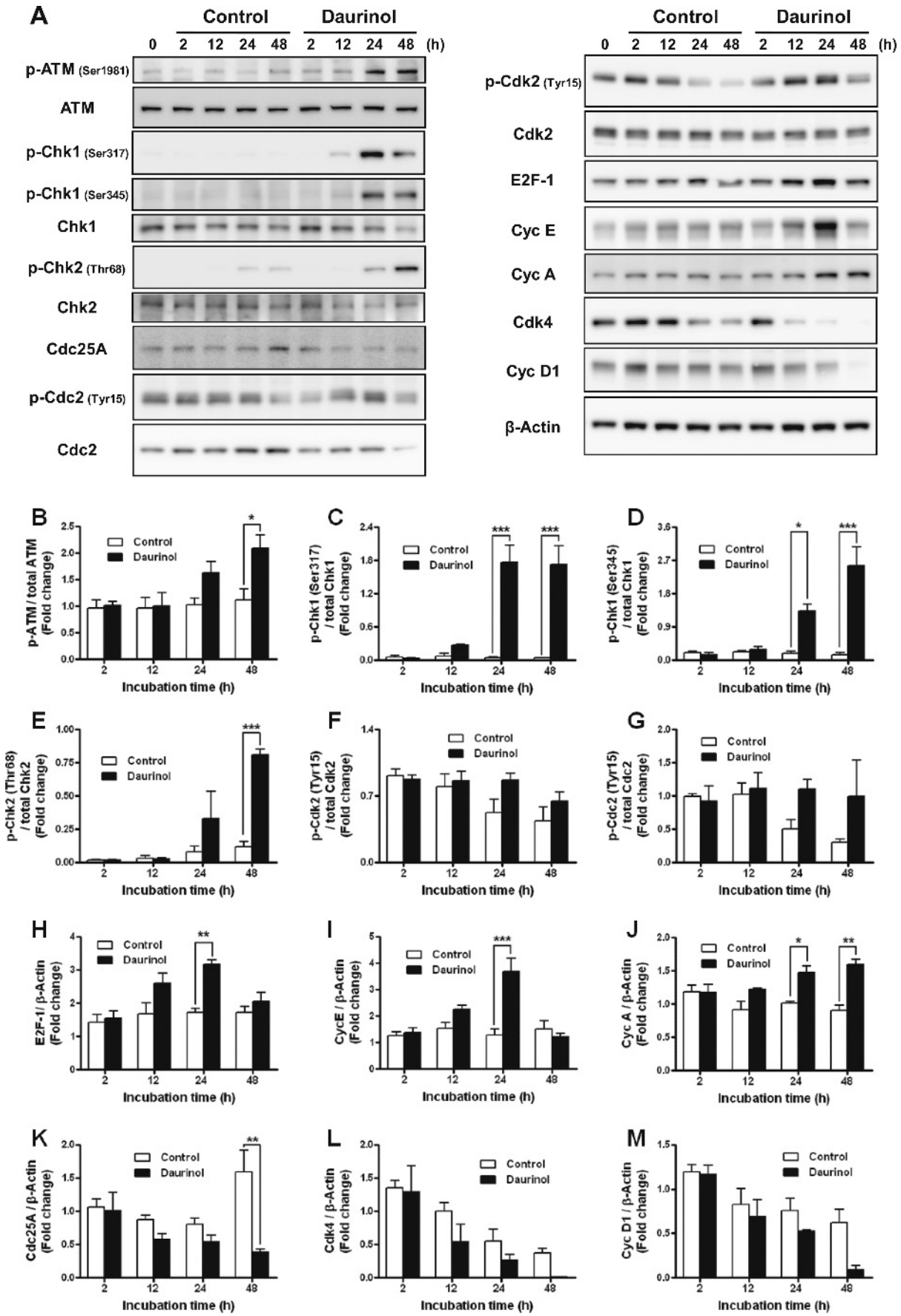
A
Control
Daurinol
0 2 12 24 48 2 12 24 48 (h)
p-ATM (Ser1981)
ATM
p-Chk1 (Ser317)
p-Chk1 (Ser345)
Chk1
p-Chk2 (Thr68)
Chk2
Cdc25A
p-Cdc2 (Tyr15)
Cdc2
p-Cdk2 (Tyr15)
Cdk2
E2F-1
Cyc E
Cyc A
Cdk4
Cyc D1
β-Actin
B p-ATM / total ATM (Fold change)
C p-Chk1 (Ser317) / total Chk1 (Fold change)
D p-Chk1 (Ser345) / total Chk1 (Fold change)
E p-Chk2 (Thr68) / total Chk2 (Fold change)
F p-Cdk2 (Tyr15) / total Cdk2 (Fold change)
G p-Cdc2 (Tyr15) / total Cdc2 (Fold change)
H E2F-1/ β-Actin (Fold change)
I CycE / β-Actin (Fold change)
J Cyc A / β-Actin (Fold change)
K Cdc25A / β-Actin (Fold change)
L Cdk4 / β-Actin (Fold change)
M Cyc D1 / β-Actin (Fold change)
Control
Daurinol
Incubation time (h)

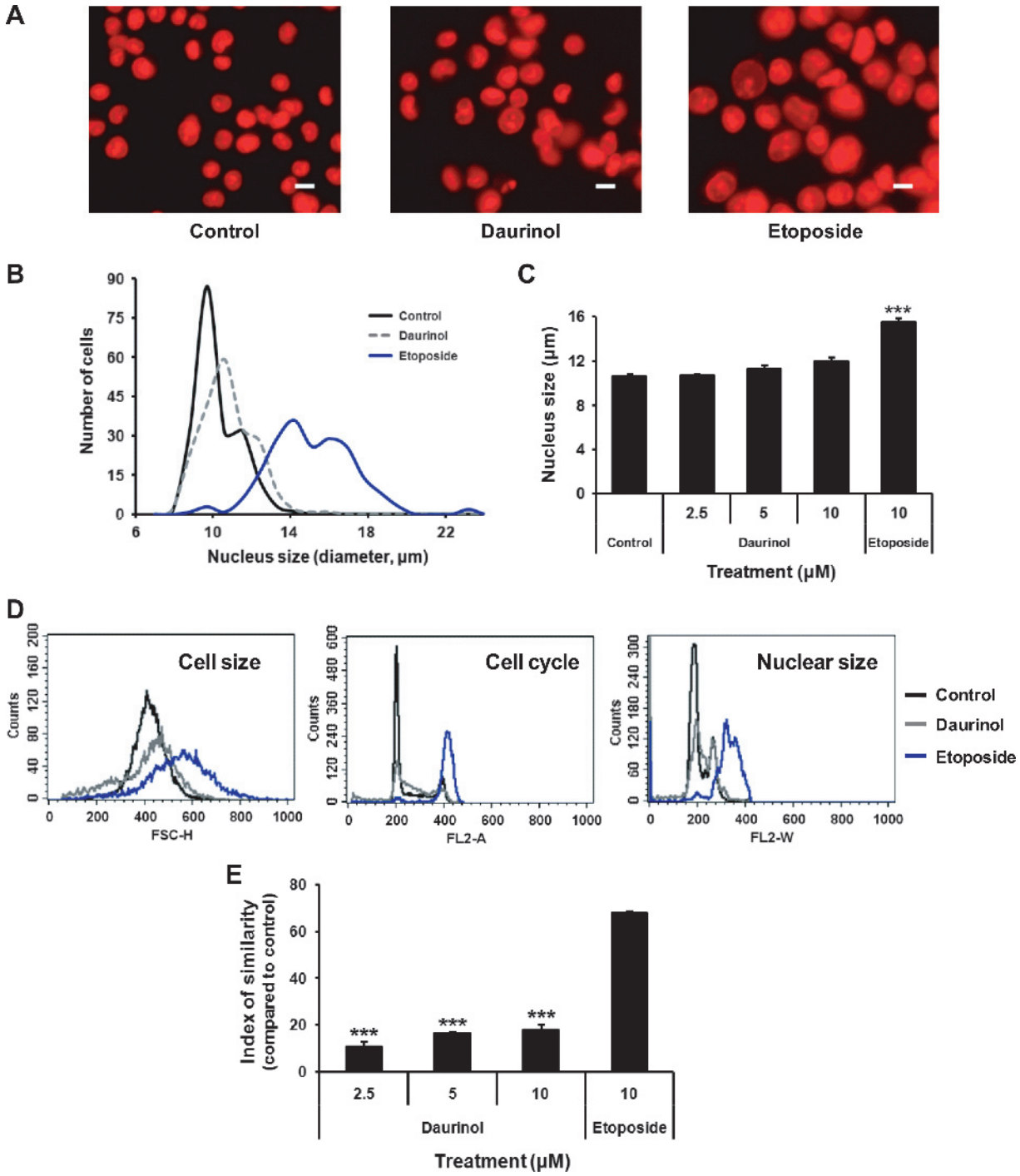

Figure 5. Effects of daurinol and etoposide on the nucleus size of HCT116 cells were evaluated by fluorescence microscopy (A–C) and flow cytometry (D and E). HCT116 cells were treated with daurinol (2.5, 5, and 10 μM) or 10 μM etoposide for 48 hours. Cellular DNA was labeled with propidium iodide for visualization and flow cytometric DNA content analysis. (A) Fluorescence microscopic images of HCT116 cells treated with 5 μM daurinol or 10 μM etoposide for 48 hours. Pictures are representative of three independent experiments (bar, 10 μm). Size of nucleus after treatment with daurinol or etoposide was determined using fluorescence microscopy and the circle measurement algorithm of the microscope software. (B) Distribution of nucleus size of HCT116 cells treated with 5 μM daurinol or 10 μM etoposide for 48 hours. (C) Mean value of nucleus diameter. Columns and error bars indicate mean ± SD (n = 200). ***P < .001, for significant differences from the vehicle control. (D) Flow cytometric analysis of HCT116 cells treated with 5 μM daurinol or 10 μM etoposide. The FSC-H, FL2-A, and FL2-W histogram plots represent cell size, cell cycle, and nucleus size, respectively. Histograms are representative of quadruplicate experiments. (E) Differences in the distributions of the FL2-W value (nucleus size) between vehicle control and chemical-treated cells were quantitatively determined using Kolmogorov-Smirnov statistics. Index of similarity is the $D/s(n)$ value of Kolmogorov-Smirnov statistics. Columns and error bars indicate mean ± SD from quadruplicate experiments. ***P < .001, for significant differences from the etoposide treatment.

first experiment was performed to evaluate the antitumor activity, toxicity, and their persistence of daurinol and etoposide treatment. Daurinol (1, 5, 10, and 20 mg/kg) or etoposide (20 mg/kg) were administered three times weekly for 2 weeks, and mice were maintained for additional 2 weeks before sacrificing. Both daurinol (1-20 mg/kg) and etoposide (20 mg/kg) displayed potent antitumor activities because the tumor volumes of all treatment groups were significantly lower than those of the vehicle-treated group (Figure 6, *B* and *D*). Tumor weights of mice treated with daurinol (5 and 20 mg/kg) or etoposide were also significantly decreased compared to the vehicle-treated group (Figure 6*C*). Importantly, the body weights of mice treated with daurinol were similar to those of vehicle-treated mice, whereas the weights of mice treated with etoposide were significantly decreased (Figure 6*A*).

A second round of *in vivo* experiments was performed to confirm antitumor activity and toxicity and to investigate changes in hematological parameters and protein expression. In these experiments, mice were treated with daurinol (5, 10, and 20 mg/kg) or etoposide (20 mg/kg) twice weekly for 3 weeks. We again found significant antitumor activity of daurinol and etoposide (Figure 7, *B* and *C*), and the body weights of mice treated with etoposide were slightly decreased compared to those of daurinol-treated and vehicle-treated mice (Figure 7*A*). The inhibition of DNA synthesis by daurinol and etoposide was also determined using BrdU immunohistochemical analysis. BrdU incorporation in mice treated with daurinol (5, 20 mg/kg) or etoposide (20 mg/kg) was significantly decreased compared to vehicle-treated mice (Figure 7*D*), and this result is consistent with our *in vitro* studies. Western blot analysis using total cell lysates prepared from xenograft tumors demonstrated activation of the ATM/Chk/Cdc25A pathway, although only the phosphorylation of Chk1 at Ser345 was significantly different (Figure 7*E*). No significant damage of normal organ tissues, including liver, kidney, and colon, was observed in either the daurinol- or etoposide-treated mice (Figure W8).

Daurinol Induces Less Hematological Damage than Etoposide in Nude Mice Xenograft Models

We investigated hematological parameters in nude mice treated with daurinol or etoposide to evaluate the hematological toxicities of the tested chemicals. White blood cell counts (WBCs) of mice treated with etoposide (20 mg/kg) were significantly lower than those of vehicle-treated mice, whereas the WBCs of mice treated with daurinol (5, 10, and 20 mg/kg) were comparable to vehicle-treated mice. Similarly, red blood cell counts (RBCs) and hemoglobin contents of mice treated with etoposide (20 mg/kg) were significantly lower than those of vehicle-treated and daurinol-treated mice. Hematocrits (%) displayed similar patterns to the results of WBCs, RBCs, and hemoglobin. Etoposide treatment significantly decreased the hematocrit (%) compared with the vehicle-treated group, whereas daurinol treatment did not, except at the 10-mg/kg dose. The number of platelets between vehicle-treated and

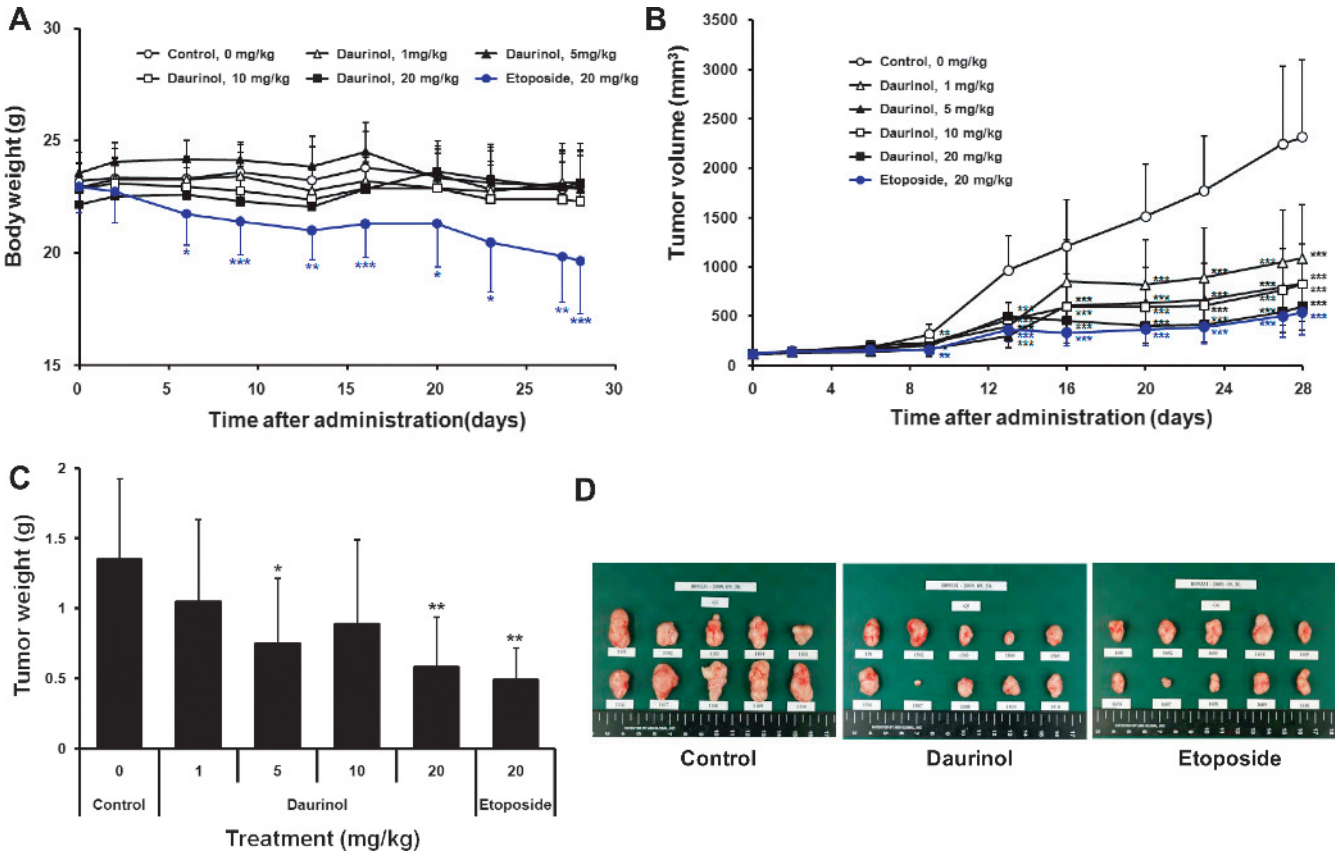

Figure 6. Antitumor activity of daurinol and etoposide in nude mice xenograft models of HCT116 cells. Daurinol (1, 5, 10, and 20 mg/kg) or etoposide (20 mg/kg) were administered intraperitoneally three times weekly for 2 weeks. Body weights (A) and tumor volumes (B) were monitored for 4 weeks after the initial injection of chemicals to evaluate toxicity, antitumor effects, and their persistence of daurinol and etoposide treatment. (C) On day 29, tumors were removed and weighed. Data are expressed as mean ± SD ($n = 10$). *$P < .05$ and **$P < .01$, for significant differences from the vehicle-treated group. (D) Photographs of tumors removed from mice treated with vehicle control, daurinol (20 mg/kg), or etoposide (20 mg/kg).

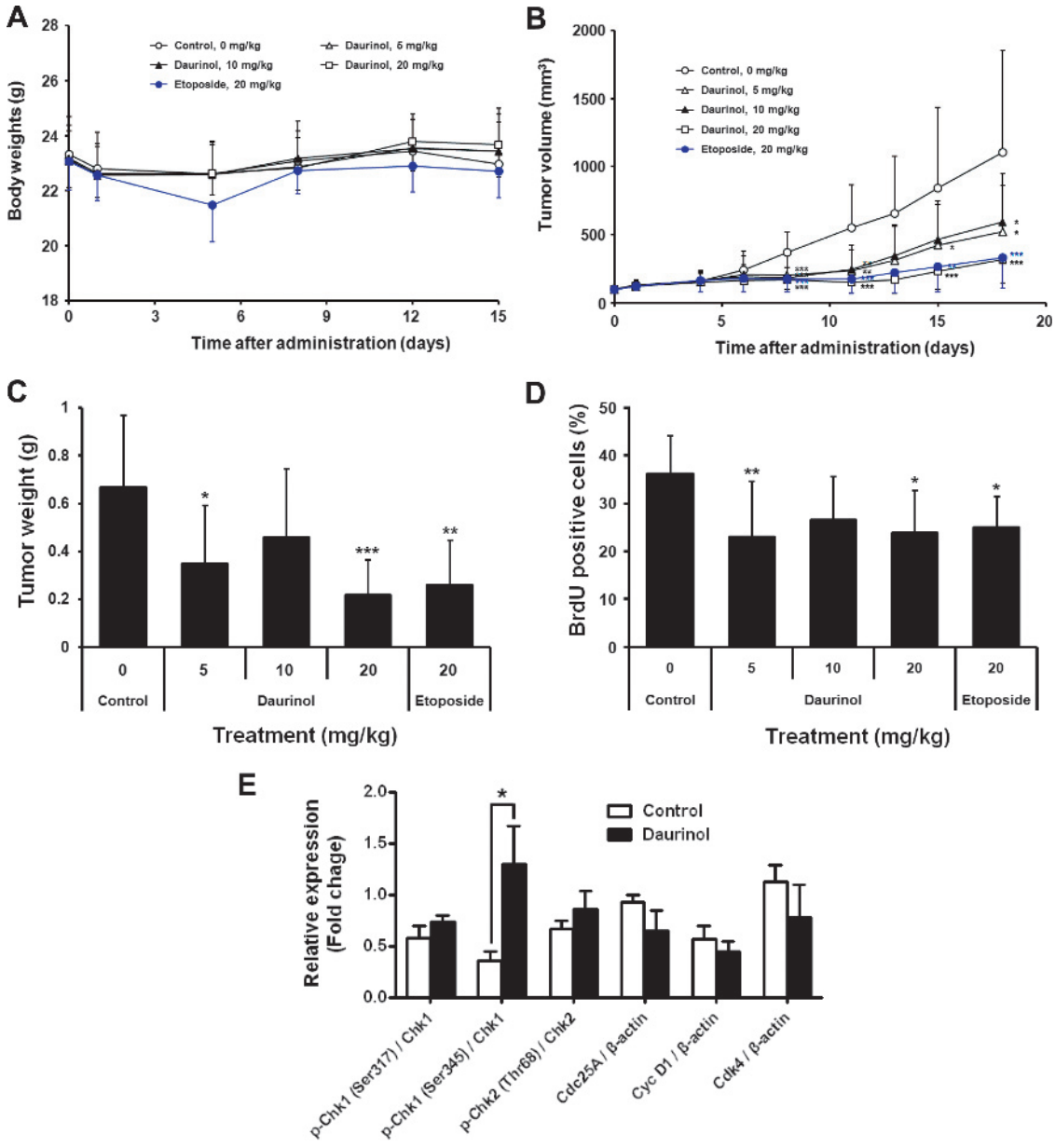

Figure 7. Evaluation of antitumor activities and molecular effects of daurinol and etoposide in nude mice xenograft models. Daurinol (5, 10, and 20 mg/kg) or etoposide (20 mg/kg) were administered intraperitoneally twice weekly for 3 weeks. Body weights (A) and tumor volumes (B) were monitored for 3 weeks. On day 18, tumors were removed for immunohistochemistry and Western blot analysis. (C) Tumor weights. (D) Inhibition of DNA synthesis in xenograft tumors was measured by BrdU incorporation immunostaining. Data are expressed as mean ± SD ($n = 10$). *$P < .05$ and **$P < .01$, for significant differences from the vehicle-treated group. (E) Western blot analysis of expression and phosphorylation of cell cycle regulatory proteins from tumors of nude mice treated with the vehicle control or daurinol (20 mg/kg). Columns and error bars indicate mean ± SEM ($n = 5$). *$P < .05$ for significant differences from the vehicle-treated group.

daurinol-treated mice was comparable, except in the 5-mg/kg daurinol treatment group. The platelet counts of mice treated with etoposide (20 mg/kg) were slightly increased compared to the vehicle-treated group (Table 1). Hematological damage was also observed by histologic examination in the bone marrow of mice treated with etoposide (Figure W8, *A–C*).

Taken together, the results of the *in vivo* experiments lead us to conclude that daurinol, a natural topoisomerase IIα inhibitor, has a potent antitumor effect in mice, with lower adverse effects, such as loss of body weight and hematological damage, compared to those induced by etoposide.

Discussion

In the present study, we report that daurinol is a promising anticancer agent that causes fewer adverse effects, such as myelosuppression, than etoposide, a well-defined clinical anticancer agent [4,13]. To demonstrate this, we investigated the similarities and differences of daurinol and etoposide in depth. Both daurinol and etoposide significantly inhibited DNA synthesis and cell viability in HCT116 human colon cancer cells. Etoposide, a human topoisomerase IIα poison, induced severe DNA damage and cell cycle arrest at G_2/M phase in HCT116 cells, whereas daurinol seems to be a catalytic inhibitor of topoisomerase IIα, which induced S-phase arrest without causing severe DNA

Table 1. Effect of Daurinol and Etoposide on the Hematological Parameters in Nude Mice Bearing HCT116 Cell Xenograft Tumors.

	Control, 0 mg/kg	Daurinol			Etoposide, 20 mg/kg
		5 mg/kg	10 mg/kg	20 mg/kg	
WBCs ($\times 10^3$ cells/μl)	4.07 ± 2.42	2.60 ± 1.12	1.86 ± 0.74	1.63 ± 0.91	0.92 ± 0.43*
RBCs ($\times 10^3$ cells/μl)	9.66 ± 0.41	9.55 ± 0.37	8.82 ± 1.20	9.24 ± 1.03	7.74 ± 0.49*
Hemoglobin (g/dl)	15.59 ± 0.61	15.33 ± 0.68	14.27 ± 1.98	14.78 ± 1.60	12.31 ± 0.76*
Hematocrit (%)	48.61 ± 2.48	47.29 ± 2.09	43.48 ± 6.38†	45.44 ± 5.34	37.36 ± 2.92*
Platelets ($\times 10^3$ cells/μl)	1418 ± 145	916 ± 457†	1220 ± 462	1091 ± 470	1733 ± 263

*$P < .001$, for significant differences from the vehicle-treated group.
†$P < .05$, for significant differences from the vehicle-treated group.

damage. Etoposide induced significant nuclear enlargement of HCT116 cells, whereas daurinol did not. We speculate that the nuclear enlargement, an abnormal chromosomal condition, could promote genomic instability of tumor tissues as well as normal tissues and may therefore be correlated with the adverse effects of etoposide. Thus, we hypothesized that daurinol might be used as a substitute anticancer agent that is less toxic to healthy tissues owing to its less severe genotoxic effects compared to etoposide. We tested this hypothesis *in vivo* with nude mice xenograft experiments. Daurinol displayed strong antitumor activity without any significant adverse effects, such as decreased body weight, blood cell counts, hemoglobin content, and hematocrit, unlike etoposide, which had significant effects on all hematological parameters. The differences between daurinol and etoposide are summarized in Figure 8*A*. Our experimental approaches, such as considering nuclear size changes *in vitro* and comparative analysis between novel candidates and old drugs, provide a practical strategy for the development of anticancer agents with decreased adverse effects.

We could not observed nuclear enlargement in the kidney and liver cells as well as actively dividing colon epithelium and bone marrow cells of nude mice treated with etoposide. This result is a typical example of discordance between *in vitro* and *in vivo* experiments. We assumed that cells with enlarged, abnormal nuclei are very dangerous to animals and may be actively eliminated in normal tissue by programmed cell death, such as apoptosis and macrophage engulfment [9]. One possible explanation is that the effective concentration of etoposide in normal tissue may be quite low compared with *in vitro* cultured cells, and therefore, it was not sufficient to induce G_2/M arrest in the animal model because of the absorption, distribution, metabolism, and/or excretion of the compound.

We also elucidated the molecular mechanism of S-phase arrest induced by daurinol treatment. Daurinol-induced S-phase arrest can be predicted by the inhibition of DNA synthesis. We found that S-phase was the rate-limiting step of the cell cycle in HCT116 cells treated with daurinol, that is, a greater number of daurinol-treated HCT116 cells were in S-phase compared to vehicle control cells. The changes in cellular signaling shown by Western blot analysis could also explain the daurinol-induced S-phase arrest in HCT116 cells. Cdk2/cyclin E and Cdk2/cyclin A complexes are involved in the initiation and progression of S-phase, respectively [33–35]. The up-regulation of cyclin E at early times (12 and 24 hours) and continued high expression of cyclin A at 12, 24, and 48 hours were observed after treatment with daurinol, indicating enhanced S-phase initiation. In addition, the expression of E2F-1 was significantly increased at 24 hours of treatment. E2F-1 is an important transcription factor regulating cell cycle control and is known to transcribe cyclin E and cyclin A [39,40]. We also examined activation of the ATM/Chk/Cdc25A pathway, which recognizes DNA damage in cells. Daurinol induced the phosphorylation of ATM at Ser 1981, Chk1 at Ser317 and Ser345, and Chk2 at Thr 68

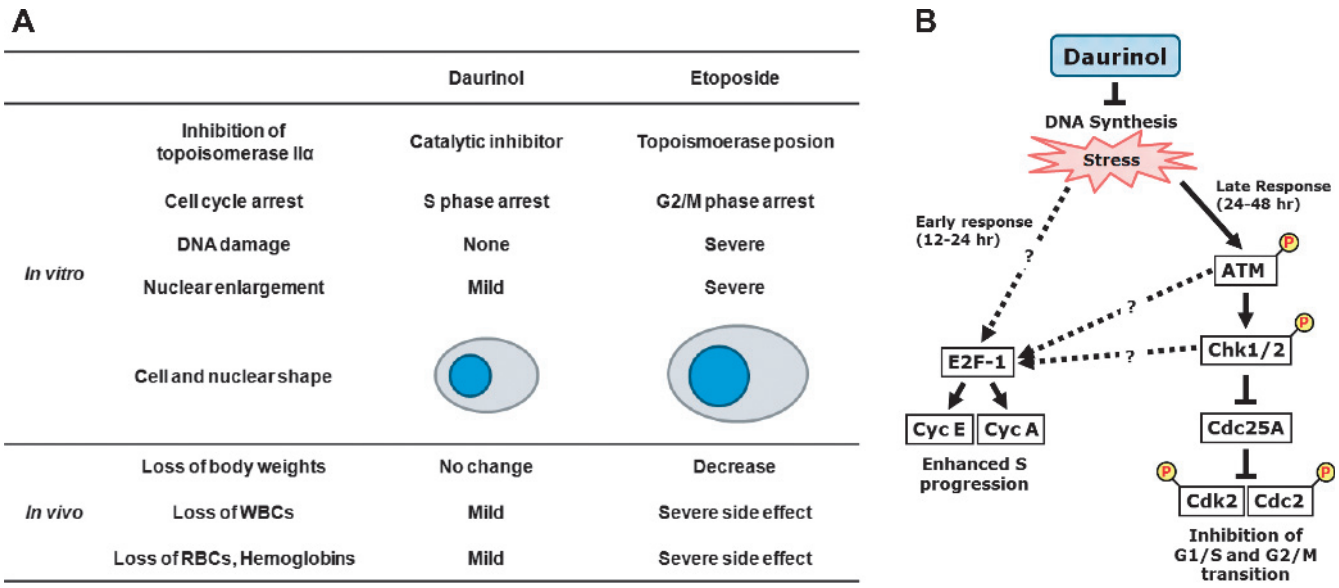

Figure 8. (A) Comparison of daurinol and etoposide. (B) Schematic representation of the possible molecular mechanism of S-phase arrest induced by daurinol treatment in human colon cancer cells.

at later time points (24–48 hours). Daurinol also induced the degradation of Cdc25A at 24 to 48 hours of treatment. Cdc25A is degraded on phosphorylation by the upstream signaling kinases Chk1 and Chk2 [33,36,37]. Cdc25A is a phosphatase that inhibits Cdk2 and Cdc2 activities by dephosphorylation at Tyr15 residue, and Cdk2 and Cdc2 are important cyclin-dependent kinases for the G_1/S and G_2/M transitions, respectively [36,38]. Daurinol also increased the phosphorylation at the Tyr 15 of Cdk2 and Cdc2 at 48 hours after treatment. These data imply that daurinol can inhibit both G_1/S and G_2/M transitions at 48 hours. Taken together, these data suggest that daurinol-induced S-phase arrest results from enhanced initiation and progression of S-phase at early times (24 hours) and the concomitant inhibition of G_1/S and G_2/M transition at later times (48 hours). A proposed model for the signaling pathway of daurinol-induced S-phase arrest is shown in Figure 8*B*.

We did not elucidate the signaling upstream of the regulation of E2F-1, cyclin E, and cyclin A in detail, but these are crucial components for understanding S-phase arrest induced by daurinol. Thus, further investigation of these pathways is needed. ATM/ATR and Chk1/2 are possible candidates because it has recently been suggested that accumulation of E2F-1 via phosphorylation by ATM/ATR and Chk1/2 may control cell cycle arrest, apoptosis, and DNA repair on DNA damage in cells [41].

In the present study, we also found that expression of the Cdk4 and cyclin D1 proteins, which are important cell cycle regulatory proteins during G_1 phase [35,42], decreased after daurinol treatment both *in vitro* and *in vivo* (Figures 4, *A*, *L,* and *M*, and 7*E*). These data also indicate that daurinol treatment inhibits the G_1 checkpoint. We postulate that moderate inhibition of each cell cycle checkpoint may contribute to the overall slowing of the cell cycle in cancer cells. We also hypothesize that the decrease of cyclin D1 may result from the inhibition of the Wnt signaling, which is an important signaling pathway in colon cancer initiation [43,44], because daurinol treatment completely inhibited mRNA expression of genes involved in the Wnt signaling pathway in HCT116 cells according to complementary DNA microarray experiments (data not shown). Therefore, we will further study the inhibitory effect of daurinol on the Wnt signaling to elucidate the cancer chemopreventive effects of daurinol.

We demonstrated that daurinol inhibits human topoisomerase IIα without the formation of the DNA cleavable complex. Thus, daurinol could be a catalytic inhibitor that interferes with at least one step of the catalytic cycle of topoisomerase. Further in-depth biochemical studies are required to identify the exact step of the enzyme cycle that is inhibited (e.g., DNA binding, ATP association/dissociation, magnesium ion binding, or dissociation from DNA) [12]. Furthermore, the inhibition of other topoisomerases, including topoisomerase I and IIβ, must also be tested to fully characterize the biochemical mechanism underlying daurinol-mediated inhibition of DNA synthesis.

The main structural difference between daurinol and etoposide is that daurinol has an arylnaphthalene moiety, whereas etoposide contains an aryltetraline moiety. The aryltertaline lignan teniposide (VM-26) and etoposide are synthetic derivatives of podophyllotoxin, a natural plant aryltetraline lignan [3]. Like etoposide, teniposide has been used to treat various human cancers, including small cell lung cancer, testicular cancer, and lymphoma [45]. Teniposide also induces G_2/M arrest and DNA damage in cancer cells [45,46] and has been reported to cause severe hematological damage, such as myelosuppression, leukopenia, and thrombopenia, in clinical cancer trails [47,48]. We propose that daurinol is a promising lead compound for the development of a novel anticancer agent that is similar to etoposide but has reduced adverse effects, including myelosuppression. Therefore, strategies are needed to synthesize or derive daurinol and to optimize its antitumor efficacy, toxicity, solubility, and pharmacokinetics.

In summary, we have shown that daurinol, a novel plant arylnaphthalene lignan, is a potential anticancer agent that causes less hematological damage than the related clinical agent etoposide. However, further studies of the molecular mechanisms of the anticancer effects of daurinol, including upstream signaling and its mode of inhibition against human topoisomerases, as well as preclinical and clinical trials of daurinol, are needed.

Acknowledgments

The authors thank Chul Young Kim (Korea Institute of Science and Technology) for helpful discussions about the natural product chemistry of arylnaphthalene lignans.

References

[1] Wang Y, Probin V, and Zhou D (2006). Cancer therapy–induced residual bone marrow injury—mechanisms of induction and implication for therapy. *Curr Cancer Ther Rev* **2**, 271–279.

[2] Kobayashi K and Ratain MJ (1994). Pharmacodynamics and long-term toxicity of etoposide. *Cancer Chemother Pharmacol* **34**, S64–S68.

[3] Baldwin EL and Osheroff N (2005). Etoposide, topoisomerase II and cancer. *Curr Med Chem Anticancer Agents* **5**, 363–372.

[4] Hande KR (1998). Etoposide: four decades of development of a topoisomerase II inhibitor. *Eur J Cancer* **34**, 1514–1521.

[5] Smith MA, Rubinstein L, Anderson JR, Arthur D, Catalano PJ, Freidlin B, Heyn R, Khayat A, Krailo M, Land VJ, et al. (1999). Secondary leukemia or myelodysplastic syndrome after treatment with epipodophyllotoxins. *J Clin Oncol* **17**, 569–577.

[6] Choudhury RC, Palo AK, and Sahu P (2004). Cytogenetic risk assessment of etoposide from mouse bone marrow. *J Appl Toxicol* **24**, 115–122.

[7] Attia SM, Al-Anteet AA, Al-Rasheed NM, Alhaider AA, and Al-Harbi MM (2009). Protection of mouse bone marrow from etoposide-induced genomic damage by dexrazoxane. *Cancer Chemother Pharmacol* **64**, 837–845.

[8] Kapiszewska M, Cierniak A, Papiez MA, Pietrzycka A, Stepniewski M, and Lomnicki A (2007). Prolonged quercetin administration diminishes the etoposide-induced DNA damage in bone marrow cells of rats. *Drug Chem Toxicol* **30**, 67–81.

[9] Enomoto R, Koshiba C, Suzuki C, and Lee E (2011). Wogonin potentiates the antitumor action of etoposide and ameliorates its adverse effects. *Cancer Chemother Pharmacol* **67**, 1063–1072.

[10] Cierniak A, Papiez M, and Kapiszewska M (2004). Modulatory effect of quercetin on DNA damage, induced by etoposide in bone marrow cells and on changes in the activity of antioxidant enzymes in rats. *Rocz Akad Med Bialymst* **49**, 167–169.

[11] Montecucco A and Biamonti G (2007). Cellular response to etoposide treatment. *Cancer Lett* **252**, 9–18.

[12] Larsen AK, Escargueil AE, and Skladanowski A (2003). Catalytic topoisomerase II inhibitors in cancer therapy. *Pharmacol Ther* **99**, 167–181.

[13] Boos G and Stopper H (2000). Genotoxicity of several clinically used topoisomerase II inhibitors. *Toxicol Lett* **116**, 7–16.

[14] Bueno C, Catalina P, Melen GJ, Montes R, Sanchez L, Ligero G, Garcia-Perez JL, and Menendez P (2009). Etoposide induces MLL rearrangements and other chromosomal abnormalities in human embryonic stem cells. *Carcinogenesis* **30**, 1628–1637.

[15] Schonn I, Hennesen J, and Dartsch DC (2010). Cellular responses to etoposide: cell death despite cell cycle arrest and repair of DNA damage. *Apoptosis* **15**, 162–172.

[16] Zhu H, Miao ZH, Huang M, Feng JM, Zhang ZX, Lu JJ, Cai YJ, Tong LJ, Xu YF, Qian XH, et al. (2009). Naphthalimides induce G(2) arrest through the ATM-activated Chk2-executed pathway in HCT116 cells. *Neoplasia* **11**, 1226–1234.

[17] Nam C, Doi K, and Nakayama H (2010). Etoposide induces G_2/M arrest and apoptosis in neural progenitor cells via DNA damage and an ATM/p53–related pathway. *Histol Histopathol* **25**, 485–493.

[18] Kang K, Lee SB, Yoo JH, and Nho CW (2010). Flow cytometric fluorescence pulse width analysis of etoposide-induced nuclear enlargement in HCT116 cells. *Biotechnol Lett* **32**, 1045–1052.

[19] Rello-Varona S, Gamez A, Moreno V, Stockert JC, Cristobal J, Pacheco M, Canete M, Juarranz A, and Villanueva A (2006). Metaphase arrest and cell death induced by etoposide on HeLa cells. *Int J Biochem Cell Biol* **38**, 2183–2195.

[20] Batsuren D, Batirov EK, Malikov VM, Zemlyanskii VN, and Yagudaev MR (1981). Arylnaphthalene lignans of *Haplophyllum dauricum*. The structure of daurinol. *Chem Nat Compd* **17**, 223–225.

[21] Graham JG, Quinn ML, Fabricant DS, and Farnsworth NR (2000). Plants used against cancer—an extension of the work of Jonathan Hartwell. *J Ethnopharmacol* **73**, 347–377.

[22] Pradheepkumar CP, Panneerselvam N, and Shanmugam G (2000). Cleistanthin A causes DNA strand breaks and induces apoptosis in cultured cells. *Mutat Res* **464**, 185–193.

[23] Navarro E, Alonso SJ, Trujillo J, Jorge E, and Perez C (2001). General behavior, toxicity, and cytotoxic activity of elenoside, a lignan from *Justicia hyssopifolia*. *J Nat Prod* **64**, 134–135.

[24] Susplugas S, Hung NV, Bignon J, Thoison O, Kruczynski A, Sevenet T, and Gueritte F (2005). Cytotoxic arylnaphthalene lignans from a Vietnamese acanthaceae, *Justicia patentiflora*. *J Nat Prod* **68**, 734–738.

[25] Kang K, Lee HJ, Kim CY, Lee SB, Tunsag J, Batsuren D, and Nho CW (2007). The chemopreventive effects of *Saussurea salicifolia* through induction of apoptosis and phase II detoxification enzyme. *Biol Pharm Bull* **30**, 2352–2359.

[26] Kang K, Jho EH, Lee HJ, Oidovsambuu S, Yun JH, Kim CY, Yoo JH, Kim YJ, Kim JH, Ahn SY, et al. (2011). *Youngia denticulata* protects against oxidative damage induced by *tert*-butyl hydroperoxide in HepG2 cells. *J Med Food* **14**, 1198–1207.

[27] Kang K, Lee SB, Jung SH, Cha KH, Park WD, Sohn YC, and Nho CW (2009). Tectoridin, a poor ligand of estrogen receptor α, exerts its estrogenic effects via an ERK-dependent pathway. *Mol Cells* **27**, 351–357.

[28] Young IT (1977). Proof without prejudice: use of the Kolmogorov-Smirnov test for the analysis of histograms from flow systems and other sources. *J Histochem Cytochem* **25**, 935–941.

[29] Smith PJ, Soues S, Gottlieb T, Falk SJ, Watson JV, Osborne RJ, and Bleehen NM (1994). Etoposide-induced cell cycle delay and arrest-dependent modulation of DNA topoisomerase II in small-cell lung cancer cells. *Br J Cancer* **70**, 914–921.

[30] Gong Y, Firestone GL, and Bjeldanes LF (2006). 3,3′-Diindolylmethane is a novel topoisomerase IIα catalytic inhibitor that induces S-phase retardation and mitotic delay in human hepatoma HepG2 cells. *Mol Pharmacol* **69**, 1320–1327.

[31] Lee BH, Yeo GY, Jang KJ, Lee DJ, Noh SG, and Cho TS (2009). A thermodynamic study on the interaction of quinolone antibiotics and DNA. *Bull Korean Chem Soc* **30**, 1031–1034.

[32] Mussardo P, Corda E, Gonzalez-Ruiz V, Rajesh J, Girotti S, Martin MA, and Olives AI (2011). Study of non-covalent interactions of luotonin A derivatives and the DNA minor groove as a first step in the study of their analytical potential as DNA probes. *Anal Bioanal Chem* **400**, 321–327.

[33] Eastman A (2004). Cell cycle checkpoints and their impact on anticancer therapeutic strategies. *J Cell Biochem* **91**, 223–231.

[34] Masai H, Matsumoto S, You Z, Yoshizawa-Sugata N, and Oda M (2010). Eukaryotic chromosome DNA replication: where, when, and how? *Annu Rev Biochem* **79**, 89–130.

[35] Weinberg RA (2007). pRB and control of the cell cycle clock. In *The Biology of Cancer*. Garland Science, New York, NY. pp. 255–366.

[36] Morgan MA, Parsels LA, Parsels JD, Mesiwala AK, Maybaum J, and Lawrence TS (2005). Role of checkpoint kinase 1 in preventing premature mitosis in response to gemcitabine. *Cancer Res* **65**, 6835–6842.

[37] Bartek J, Lukas C, and Lukas J (2004). Checking on DNA damage in S phase. *Nat Rev Mol Cell Biol* **5**, 792–804.

[38] Ray D and Kiyokawa H (2007). CDC25A levels determine the balance of proliferation and checkpoint response. *Cell Cycle* **6**, 3039–3042.

[39] DeGregori J, Kowalik T, and Nevins JR (1995). Cellular targets for activation by the E2F1 transcription factor include DNA synthesis- and G_1/S-regulatory genes. *Mol Cell Biol* **15**, 4215–4224.

[40] Helin K (1998). Regulation of cell proliferation by the E2F transcription factors. *Curr Opin Genet Dev* **8**, 28–35.

[41] Stevens C and La Thangue NB (2004). The emerging role of E2F-1 in the DNA damage response and checkpoint control. *DNA Repair (Amst)* **3**, 1071–1079.

[42] Diehl JA (2002). Cycling to cancer with cyclin D1. *Cancer Biol Ther* **1**, 226–231.

[43] Yoo JH, Lee HJ, Kang K, Jho EH, Kim CY, Baturen D, Tunsag J, and Nho CW (2010). Lignans inhibit cell growth via regulation of Wnt/β-catenin signaling. *Food Chem Toxicol* **48**, 2247–2252.

[44] Barker N and Clevers H (2006). Mining the Wnt pathway for cancer therapeutics. *Nat Rev Drug Discov* **5**, 997–1014.

[45] Botta B, Delle Monache G, Misiti D, Vitali A, and Zappia G (2001). Aryltetralin lignans: chemistry, pharmacology and biotransformations. *Curr Med Chem* **8**, 1363–1381.

[46] Chen M and Beck WT (1995). Differences in inhibition of chromosome separation and G_2 arrest by DNA topoisomerase II inhibitors merbarone and VM-26. *Cancer Res* **55**, 1509–1516.

[47] Hartmann JT and Lipp HP (2006). Camptothecin and podophyllotoxin derivatives: inhibitors of topoisomerase I and II—mechanisms of action, pharmacokinetics and toxicity profile. *Drug Saf* **29**, 209–230.

[48] Cascinu S, Del Ferro E, Ligi M, Graziano F, and Catalano G (1997). The clinical impact of teniposide in the treatment of elderly patients with small-cell lung cancer. *Am J Clin Oncol* **20**, 477–478.

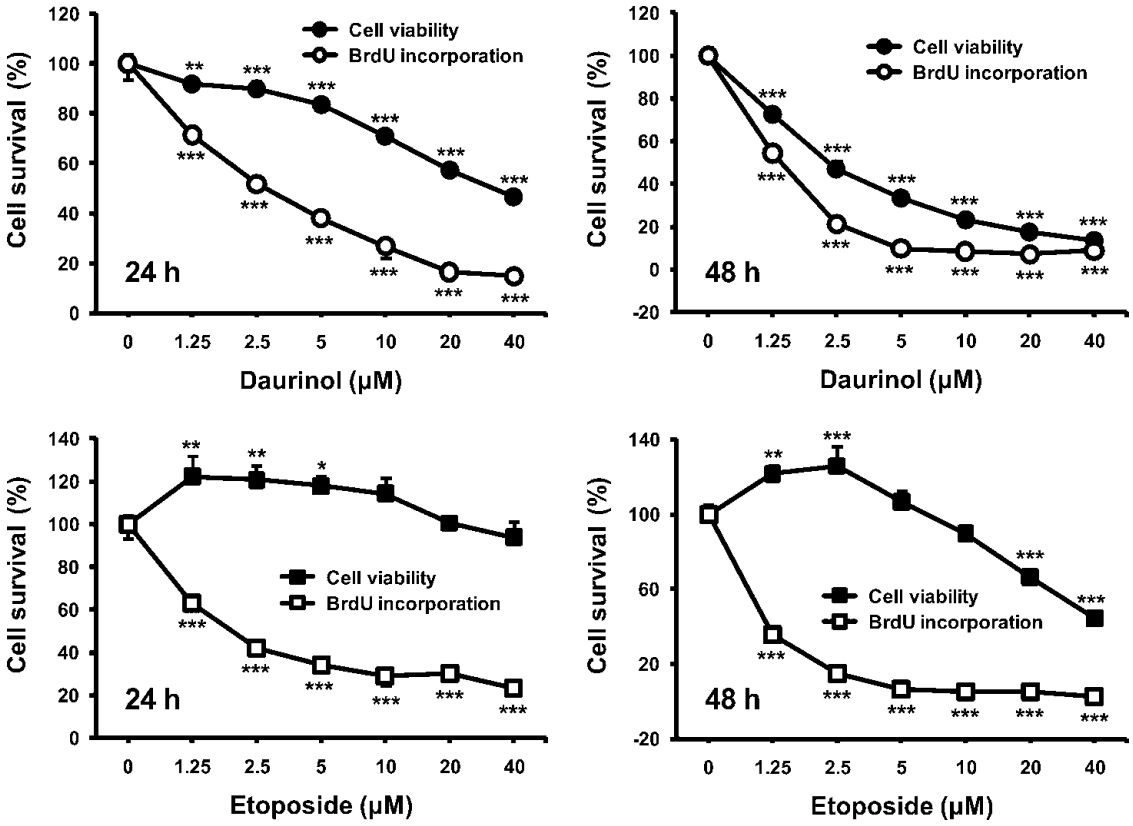

Figure W1. Daurinol inhibits both cell viability (mitochondrial dehydrogenase activity) and DNA synthesis (BrdU incorporation) in human colon cancer DLD-1 cells. Cell survival after treatment with daurinol or etoposide for 24 and 48 hours was determined by CCK-8 assay and BrdU incorporation ELISA in DLD-1 cells. Data are expressed as mean ± SD from triplicate experiments. $*P < .05$, $**P < .01$, and $***P < .001$, for significant differences from the vehicle control.

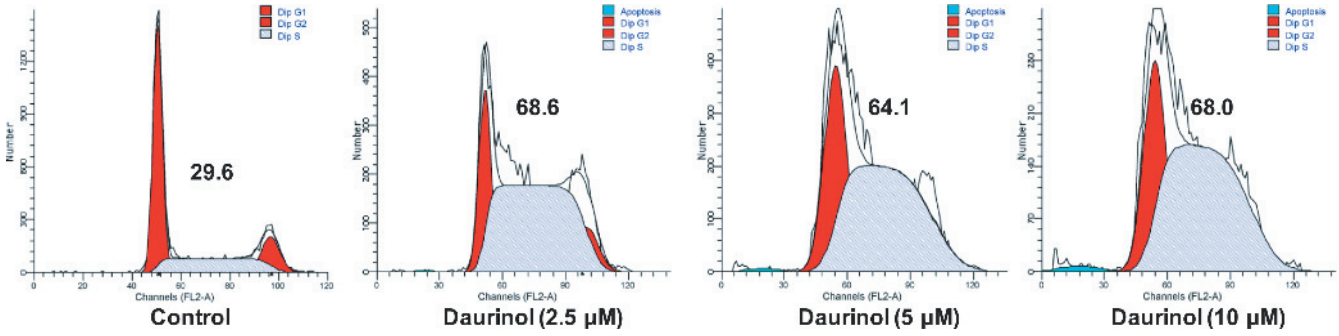

Figure W2. Daurinol induces S-phase arrest in DLD-1 cells. The cell cycle was evaluated by flow cytometric DNA content analysis. DLD-1 cells were treated with 0 to 10 μM daurinol for 48 hours. The percentage of cells in S-phase is indicated on each graph. The graph is representative of at least three independent experiments.

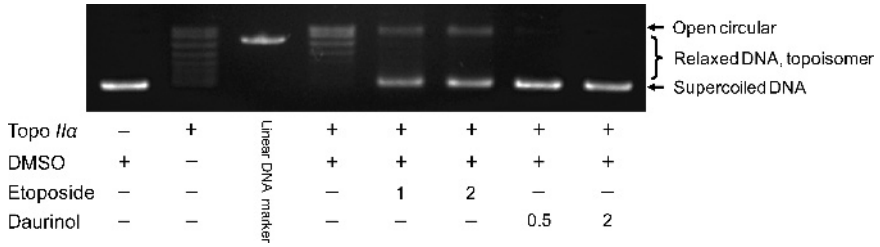

Figure W3. Daurinol inhibits human topoisomerase IIα activity. Inhibitory activity of daurinol and etoposide on human topoisomerase IIα was evaluated by *in vitro* biochemical assay using a TopoGEN kit. The supercoiled DNA (pHOT1) substrate was reacted with human topoisomerase IIα in the presence of daurinol (1 and 2 mM) or etoposide (0.5 and 2 mM). DNA relaxation was evaluated by agarose gel electrophoresis in the absence of ethidium bromide.

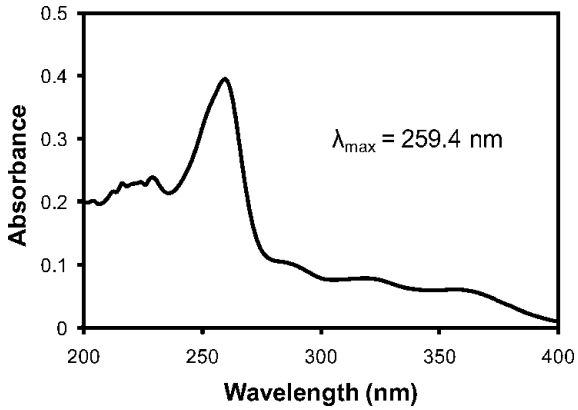

Figure W4. Absorption spectrum of 10 μM daurinol dissolved in DPBS.

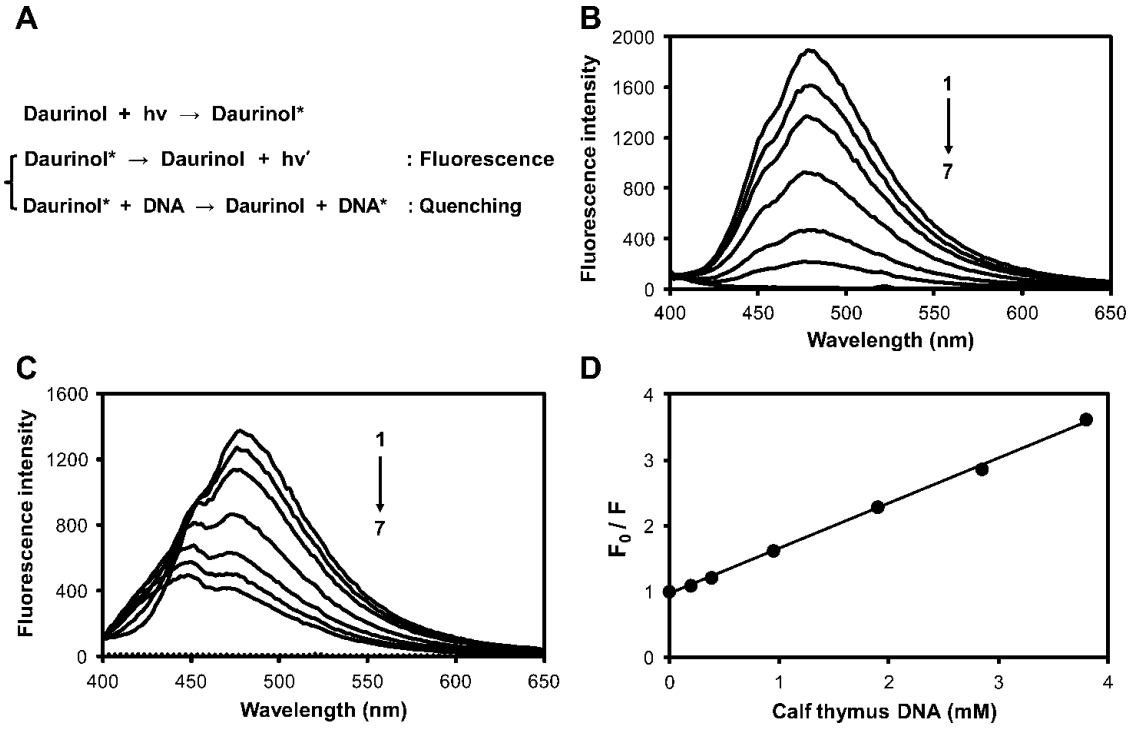

Figure W5. Daurinol interacts with DNA. The interaction of daurinol and calf thymus DNA was evaluated through fluorescence spectroscopy. (A) Theoretical chemical equation of daurinol fluorescence quenching by interaction with DNA. (B) Fluorescence emission spectrum of daurinol (λ_{ex} = 260 nm). Daurinol (50, 40, 30, 20, 10, 5, or 0 μM) was dissolved in DPBS with 2% DMSO (1–7, respectively). The graph is representative of three independent experiments. (C) Fluorescence emission spectra of 30 μM daurinol in DPBS with increasing concentration of calf thymus DNA (from 1 to 7: 0.19, 0.38, 0.95, 1.90, 2.85, or 3.80 mM) (λ_{ex} = 260 nm). DNA (3.8 mM) without daurinol did not emit fluorescence (dotted line). The graph is representative of four independent experiments. (D) Stern-Volmer plot of daurinol fluorescence quenching with increasing concentrations of calf thymus DNA. The excitation wavelength was 260 nm, and the monitoring wavelength was 480 nm at room temperature. The graph is representative of four independent experiments.

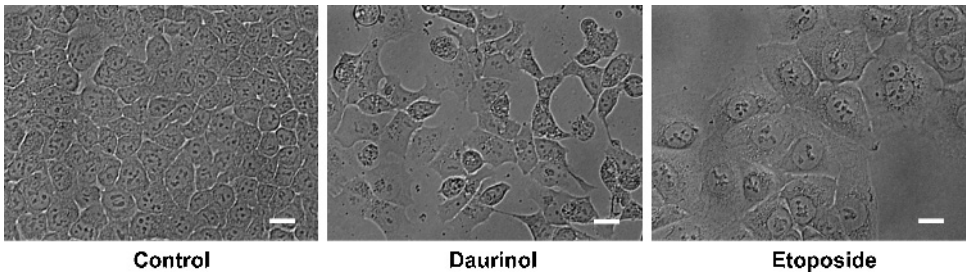

Figure W6. Differential interference contrast microscope images of HCT116 cells treated with 5 μM daurinol or 10 μM etoposide for 48 hours (bar, 20 μm).

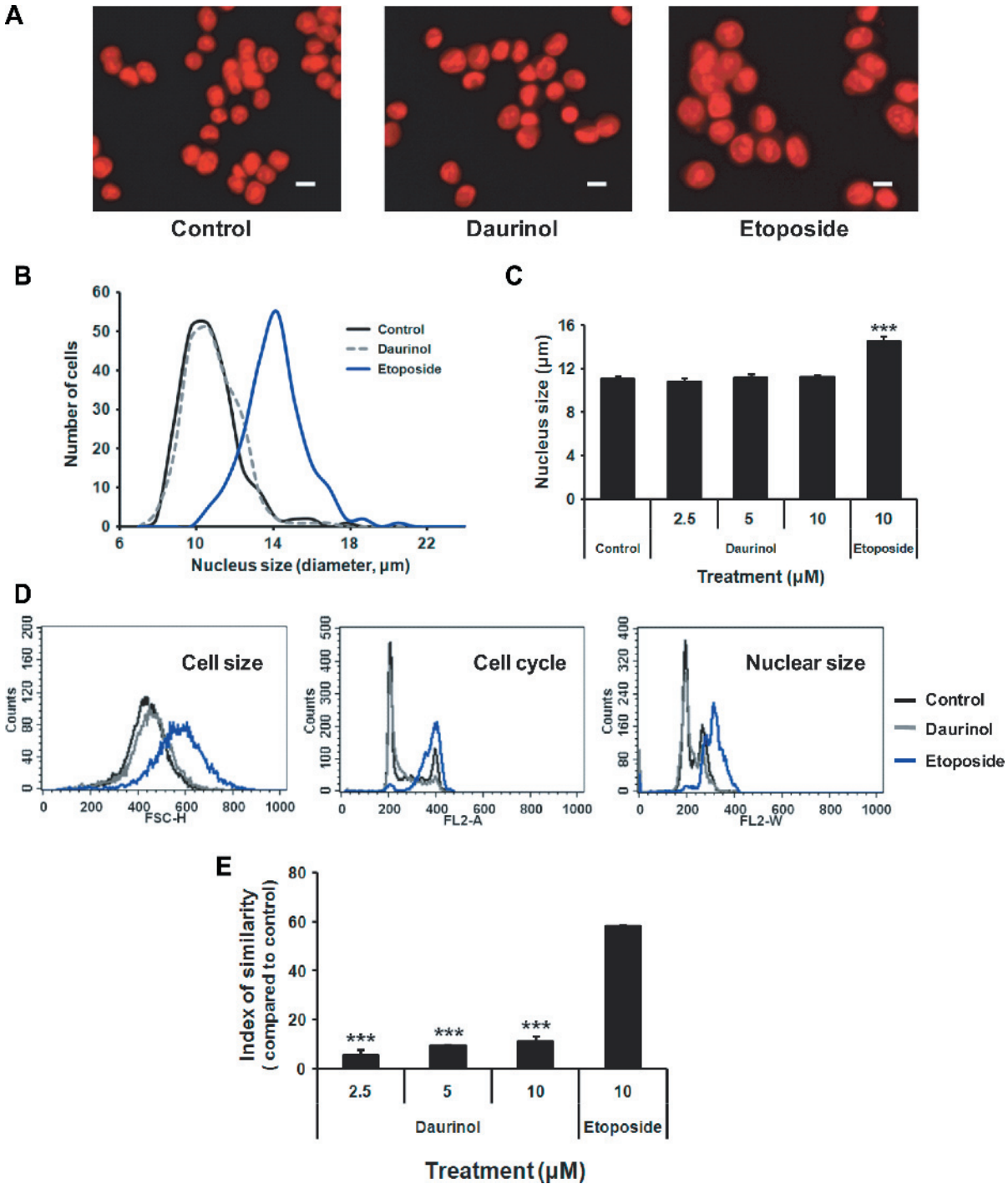

Figure W7. The effects of daurinol and etoposide on the nuclear size of HCT116 cells were evaluated by fluorescence microscopy (A–C) and flow cytometry (D and E). HCT116 cells were treated with daurinol (2.5, 5, and 10 μM) or 10 μM etoposide for 24 hours. Cellular DNA was stained with propidium iodide for visualization and flow cytometric DNA content analysis. (A) Fluorescence microscopic images of HCT116 cells treated with 5 μM daurinol or 10 μM etoposide for 24 hours. Pictures are representative of three independent experiments (bar, 10 μm). Nucleus size after treatment with daurinol or etoposide was determined by fluorescence microscopy and the circle measurement algorithm of the microscope software. (B) Distribution of nuclear size in HCT116 cells treated with 5 μM daurinol or 10 μM etoposide. (C) Mean diameter of nuclei. Columns and error bars indicate mean ± SD ($n = 200$). ***$P < .001$, for significant differences from the vehicle control. (D) Flow cytometric analysis of HCT116 cells treated with 5 μM daurinol or 10 μM etoposide for 24 hours. FSC-H, FL2-A, and FL2-W histogram plots represent cell size, cell cycle, and nucleus size, respectively. Histograms are representative of quadruplicate experiments. (E) Differences in the distribution of the FL2-W values (nucleus size) between vehicle control and chemical-treated cells were quantitatively determined using Kolmogorov-Smirnov statistics. The index of similarity is the $D/s(n)$ value of the Kolmogorov-Smirnov statistics. Columns and error bars indicate mean ± SD from quadruplicate experiments. ***$P < .001$, for significant differences from the etoposide treatment.

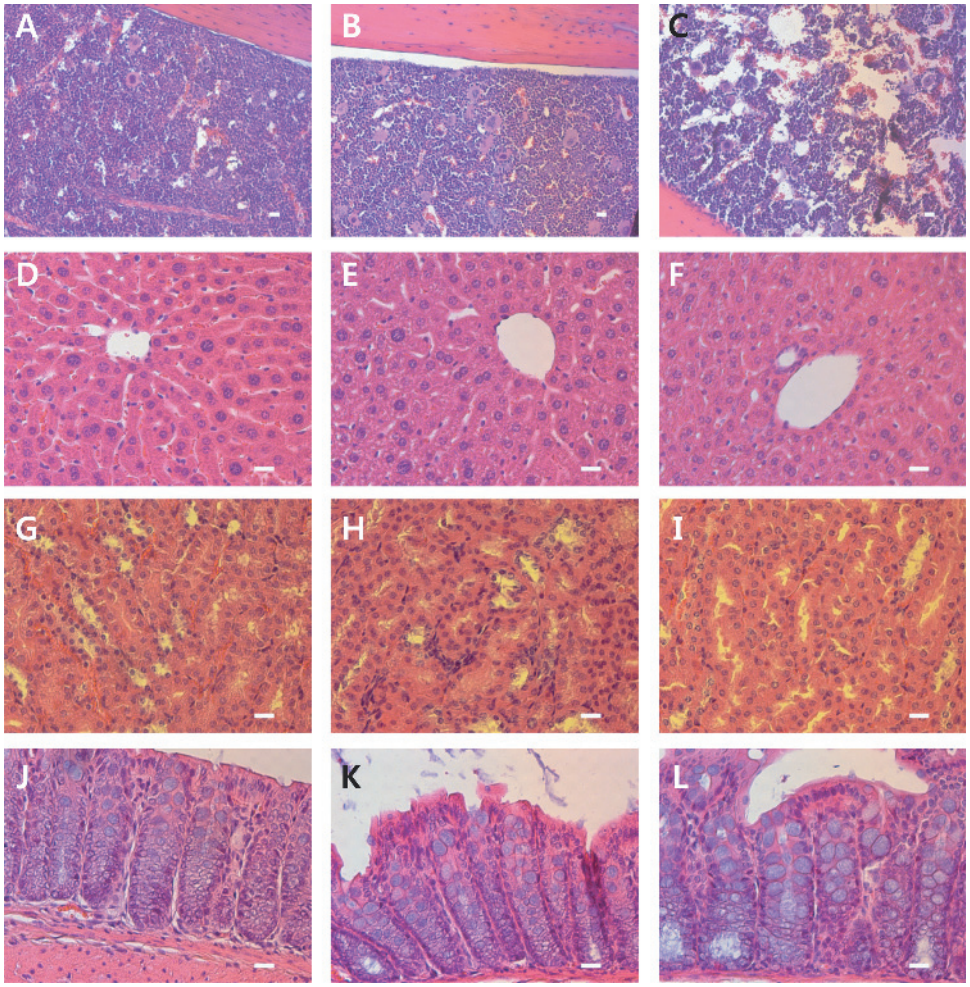

Figure W8. Effect of daurinol and etoposide on normal tissues of nude mice. Organs were removed from mice of each group after intraperitoneal injection of vehicle control, 20 mg/kg daurinol, or 20 mg/kg etoposide twice weekly for 3 weeks. Paraffin-embedded sections were stained with hematoxylin and eosin ($n = 10$). (A) Bone marrow of vehicle-treated mice. (B) Bone marrow of daurinol-treated mice. (C) Bone marrow of etoposide-treated mice. (D) Liver of vehicle-treated mice. (E) Liver of daurinol-treated mice. (F) Liver of etoposide-treated mice. (G) Kidney of vehicle-treated mice. (H) Kidney of daurinol-treated mice. (I) Kidney of etoposide-treated mice. (J) Colon of vehicle-treated mice. (K) Colon of daurinol-treated mice. (L) Colon of etoposide-treated mice (bar, 20 μm).